Southeastern Geology: Volume 41, No. 4 March 2003

Editor in Chief: S. Duncan Heron, Jr.

Abstract

Academic journal published quarterly by the Department of Geology, Duke University.

SOUTHEASTERN GEOLOGY

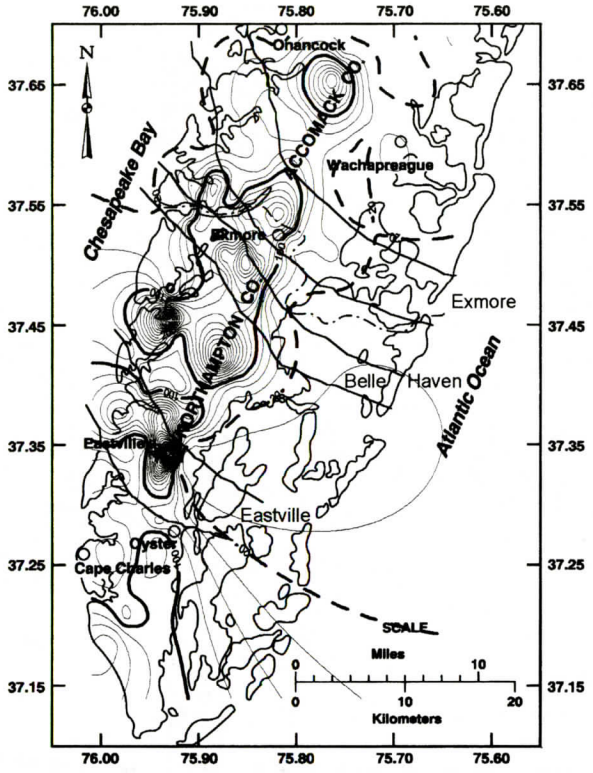

VOL. 41, NO. 4 MARCH 2003

SOUTHEASTERN GEOLOGY

Table of Contents

Volume 41, No. 4 March 2003

SOUTHEASTERN GEOLOGY

PUBLISHED

at

DUKE UNIVERSITY

Editor in Chief:

Duncan Heron

This journal publishes the results of original research on all phases of geology, geophysics, geochemistry and environmental geology as related to the Southeast. Send manuscripts to **DUNCAN HERON, DUKE UNIVERSITY, DIVISION OF EARTH & OCEAN SCIENCES, BOX 90233, DURHAM, NORTH CAROLINA 27708-0233**. Phone: 919-684-5321, Fax: 919-684-5833, Email: duncan.heron@duke.edu Please observe the following:

1) Type the manuscript with double space lines and submit in duplicate.
2) Cite references and prepare bibliographic lists in accordance with the method found within the pages of this journal.
3) Submit line drawings and complex tables reduced to final publication size (no bigger than 8 x 5 3/8 inches).
4) Make certain that all photographs are sharp, clear, and of good contrast.
5) Stratigraphic terminology should abide by the North American Stratigraphic Code (American Association Petroleum Geologists Bulletin, v. 67, p. 841-875).

Subscriptions to *Southeastern Geology* for volume 41 are: individuals - $22.00 (paid by personal check); corporations and libraries - $28.00; foreign $34. Inquires should be sent to: **SOUTHEASTERN GEOLOGY, DUKE UNIVERSITY, DIVISION OF EARTH & OCEAN SCIENCES, BOX 90233, DURHAM, NORTH CAROLINA 27708-0233**. Make checks payable to: *Southeastern Geology.*

Information about SOUTHEASTERN GEOLOGY is on the World Wide Web including a searchable author-title index 1958-2001 (Acrobat format). The URL for the Web site is:

http://www.southeasterngeology.org

SOUTHEASTERN GEOLOGY is a peer review journal.

ISSN 0038-3678

SOUTHEASTERN GEOLOGY
V. 41, No. 4, March 2003, p. 177-199

PALEOCHANNELS AND WATER RESOURCES OF THE EASTERN SHORE OF VIRGINIA: A CASE STUDY BY ELECTRICAL RESISTIVITY METHODS

ALI A. NOWROOZI, ADAM T. KARST AND PETER N. HENDERSON

Department of Ocean, Earth, and Atmospheric Sciences
Old Dominion University, Norfolk, VA 23529

ABSTRACT

Three Paleochannels are identified in the underlying Pleistocene sediments beneath the Eastern Shore of Virginia. We conducted 109 Schlumberger resistivity soundings and 25 Wenner resistivity profiles to find the shapes and boundaries of the Paleochannels using electrical resistivity methods. Results of the Wenner resistivity profiles at electrode spacings of 20, 40, and 60 meters indicate a relative increase in apparent resistivity across the Paleochannels' boundaries due to the coarser lithologies within them. Contour maps of the modeled depth to the 70, 100, and 150 ohm-m surfaces are deepening within the paths of the Paleochannels indicating the geometry of the channel. Contour maps of the modeled resistivity at depths from 20 to 70 meters below the ground surface (BGS) show increasing resistivities toward the center of the Paleochannels, again indicating coarser channel fill material. At 60 meters BGS, all three Paleochannels are detected as northwest-southeast trending elliptical anomalies having modeled resistivities of 100 to 240 ohm-m near their central axes. Our findings are roughly consistent with the land tracks of Exmore and Eastville Paleochannels previously proposed by onshore drilling and offshore seismic data. However, we obtained a slightly different track for the Belle Haven Paleochannel than previously proposed. Furthermore, our data suggests that Belle Haven is possibly a tributary of the Exmore Paleochannel; all three Paleochannels contain relatively high true resistivity layers indicating freshwater within the Paleochannels strata. However, in coastal areas, low true resistivity layers at shallow depths (20 to 30 meters BGS) within the Paleochannel boundaries and at greater depths (70 to 90 meters BGS) outside the Paleochannel boundaries indicate brackish or saltwater intrusion. The Exmore and the Belle Haven Paleochannels are within the outer and inner rim of a 35.5 million year old Chesapeake impact structure respectively, and the Eastville Paleochannel appears to be within the deeper inner rim structure. However, resistivity anomalies related to the deep impact structure are not resolved.

INTRODUCTION

Multiple Pleistocene Paleochannels lie beneath the southern Delmarva Peninsula of Virginia. They represent the main channel of the Susquehanna River during several episodes of sea level low stands which occurred, approximately 430,000 to 18,000 years ago. Subsequent filling of the channels during rises in sea level produced fining upward sequences (Coleman and Mixon, 1988, Coleman et al., 1990). The channels were formed well after the 35.5 million year old Chesapeake impact structure, Poag (1996, 1997, 2002), Johnson and others (1998), Powars and Scott (1999) and Powars (2000). Figure 1 presents the approximate positions of the channels and the outer and inner ring structures of the impact structures.

The positions of channels are known from some onshore borehole data analyzed by Mixon (1985) and the seismic reflection-profiles in the Chesapeake Bay and Atlantic Ocean analyzed by several authors (Coleman and Mixon 1988; Coleman et al. 1990; Foyle and Oertel, 1992; and Foyle, 1994). Channels passing onshore are named for towns near their boundaries. Exmore, Eastville, and Belle Haven channels are near towns by the same names. Also, Figure 1 shows the modern tidal channel of the Chesa-

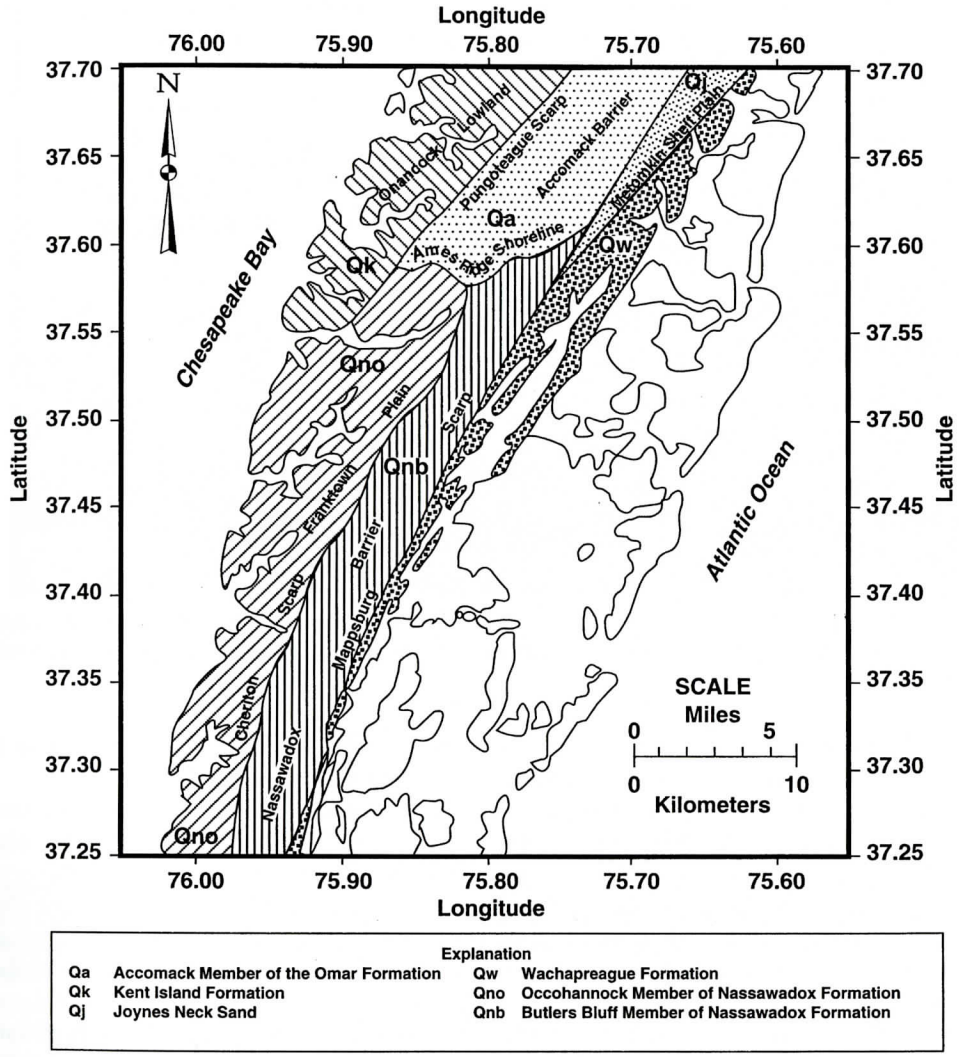

Explanation

Qa	Accomack Member of the Omar Formation	Qw	Wachapreague Formation
Qk	Kent Island Formation	Qno	Occohannock Member of Nassawadox Formation
Qj	Joynes Neck Sand	Qnb	Butlers Bluff Member of Nassawadox Formation

Figure 2. The surface geology map of the survey area, modified from Mixon (1985).

Coarse sand and gravel within the Paleochannels represent areas of higher permeability and porosity, thus, mapping their locations is important for understanding their effect on contaminant movement, groundwater modeling and hydrogeology of the area. Additionally, with their proximity to the towns of Eastville, Exmore, and Belle Haven, where ground water withdrawals are relatively high, the Paleochannels may become linked to salt water intrusion (Nowroozi et al., 1999).

Geology of the study area

The Delmarva Peninsula is part of the Atlantic Coastal Plain province and separates the Chesapeake Bay from the Atlantic Ocean. The peninsula is a low-elevation Pleistocene upland with maximum elevations of 20 meters above sea level, but in the surveyed areas is nearly flat. The central upland of the peninsula is bordered on the east and west by Pleistocene and Holocene terraces that gently slope toward the Chesapeake Bay and the Atlantic Ocean (Harrison et al., 1965; Hansen, 1966; Harrison, 1972;

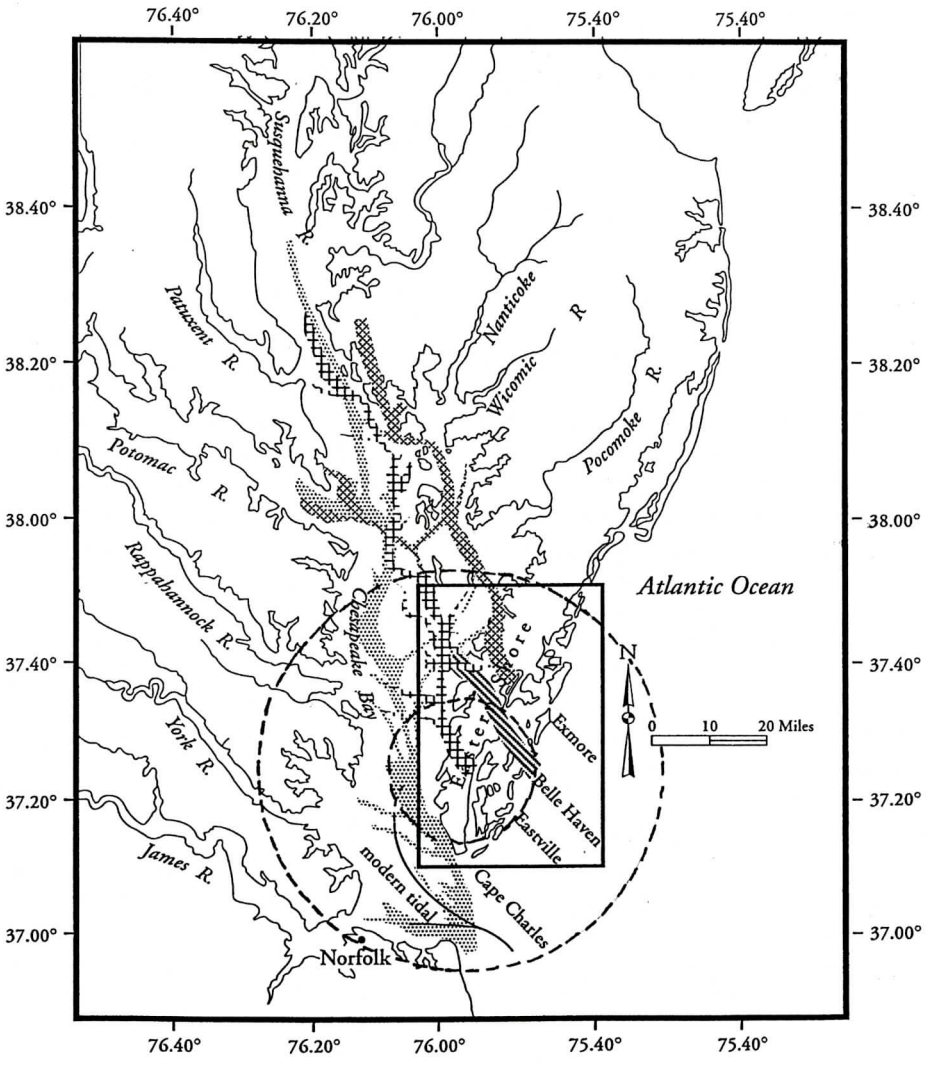

Figure 1. Location map of the study area. The insert shows the proposed locations of the Exmore, Belle Haven and Eastville Paleochannels by different patterns. The dotted pattern shows the modern channel. The approximate position of the outer and the inner rims of the Chesapeake Bay impact crater are shown by two circles from Powars and Scott, 1999.

peake Bay and Cape Charles Paleochannels, but they are not of interest in this study.

The stratigraphic sequence within the Paleochannels consists of basal gravel fining upward to estuaries' deposits capped by a barrier-spit complex. The widths of these channels are 2 to 6 km wide; their depth is 30 to 60 meters cutting into the underlying Tertiary strata, and they trend northwest to southeast (Mixon, 1985). The Paleochannels decrease in age from north to south (Coleman et al., 1990).

We used electrical resistivity to delineate the onshore geometry of the Paleochannels based on the expected contrasts in electrical properties between the coarser Quaternary channel-fill sequences and the surrounding finer-grained Tertiary deposits. This method is used worldwide at a number of sites to map buried stream channels (Zohdy et al., 1974; Darwin 1988; Donohue, 1989; El-Gamili et al., 1994).

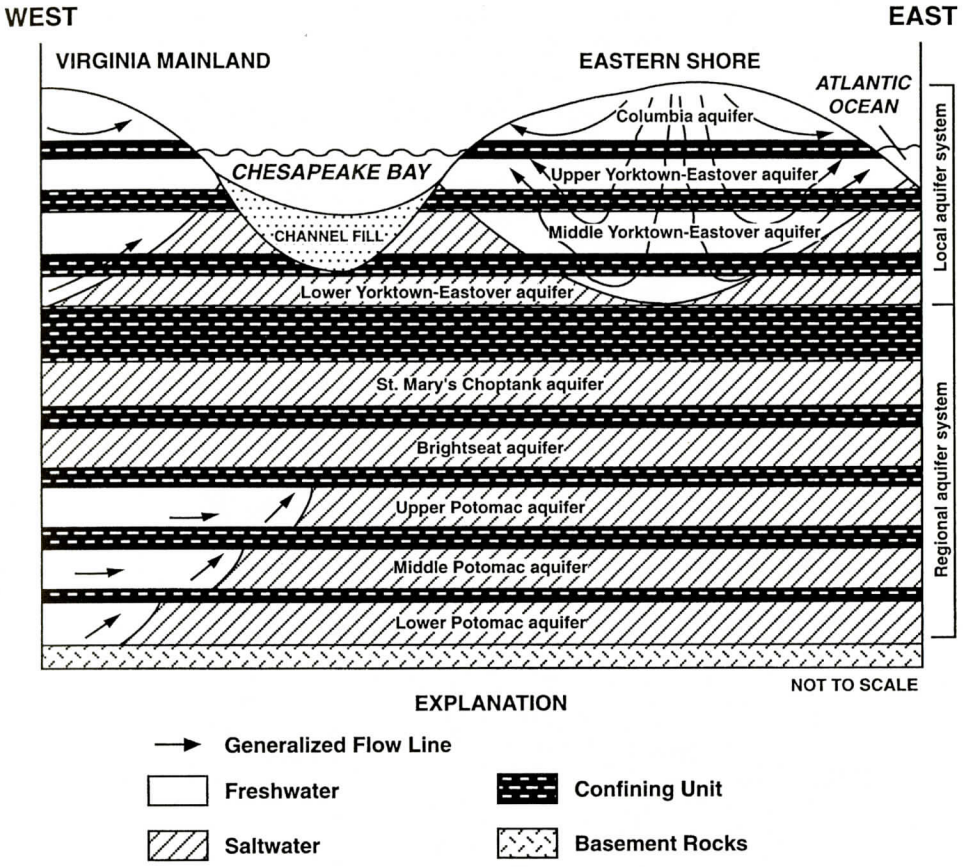

Figure 4. A schematic diagram of aquifers and generalized flow lines of the Eastern Shore from Richardson 1992; the Columbia, upper, middle and lower Yorktown-Eastover aquifers are main sources of freshwater in the Eastern Shore. They are not disturbed by the 35 million years ago impact structure.

ly. The depth to lower Potomac is not well known, it may exceed 640 meters, this system in the Eastern Shore contains saltwater also, (Richardson, 1992).

Field Work

One hundred and nine Schlumberger resistivity soundings were deployed in and around the estimated boundaries of the Paleochannels proposed by Coleman et al. (1990) and Foyle (1994). Figure 5 shows the proposed Paleochannel boundaries, the locations of the 109 soundings, the outer and inner rim of the impact structure, and the positions of borehole J-24 and CH-11 of United States Geological Survey, (Mixon, 1985). For most soundings the AB/2 spacing were at 1, 1.5, 2, 3, 5, 7, 10, 12, 16, 20, 24, 30, 40, 50, 60, 80, 100, 120, 150, 200, 250 meters respectively. The potential spacing, MN/2, initially was 0.2 m. The resistivity survey was continued until potential drops were about 0.1 mV. Then MN/2 was increased to 5 m. Usually, two points with previous AB/2 were re-surveyed using the new MN/2 spacing. The resistivity survey was then continued until a potential drop was again near 0.1 mV; then MN/2 was increased again to a new value of 10 m, and two new previous points were again re-surveyed. Always AB/2 spacing remained more than five times MN/2 spacing; thus, the recommended ratio for the Schlumberger array was always maintained. As a result of changing the MN/2 spacing, the observed field curve was

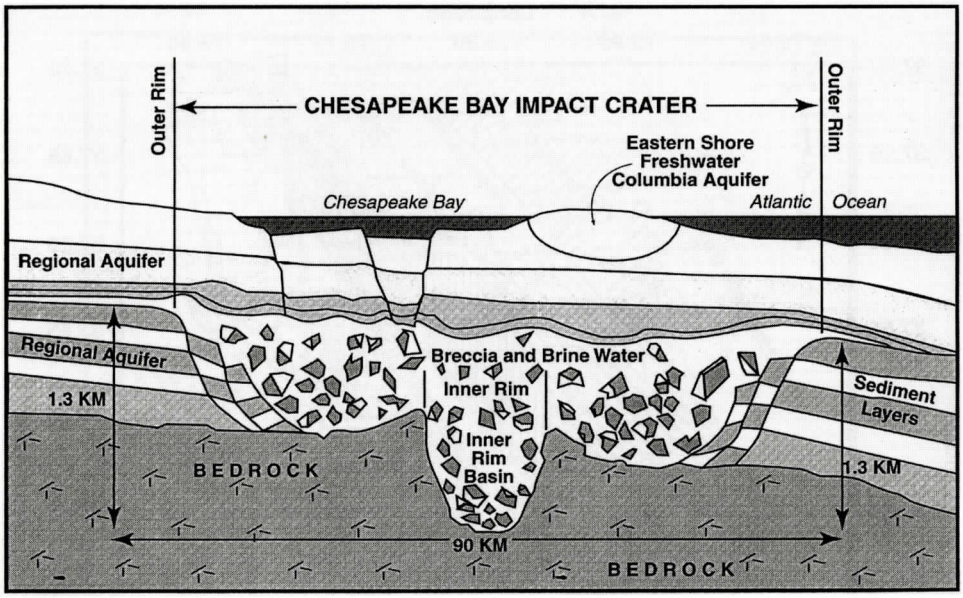

Figure 3. A cross section of the Chesapeake impact crater, modified from Poag, 1997 and 2002. The schematic position of the local freshwater lens is also shown; for other aquifer systems refer to Figure 4.

Mixon, 1985). A Holocene barrier-lagoon system separates the eastern side of the peninsula from the Atlantic Ocean. The stratigraphy of the study area consists of Cretaceous to Holocene, consolidated and unconsolidated clastic sediments that gently dip and thicken eastward (Foyle and Oertel, 1992). Quaternary sediments unconformably overly Tertiary glauconitic sand and silt; they overly a basement of Precambrian to Jurassic rocks (Mixon, 1985). Figure 2 shows the Quaternary deposits in the study area based on Mixon (1985). He collected data from about 40 boreholes in the entire Eastern Shore. They indicate up to 12 distinct layers in the upper 100 meters altitudes.

The Chesapeake bolide structure formed by the impact of an astronomical body (meteorites, asteroids or comets) about 35.5 Million years ago. The center of the impact is near present day Cape Charles in the Eastern Shore of Virginia. The faulted outer rim of the impact crater has a circular shape with a diameter of 90 km; the maximum relief of the rim to the floor is about 1.3 km. The thickness of sediments above the impact structures is 300 to 500 meters, (Poag, 1996). Thus, the 30 to 60 meters deep Paleochannels are within the sediments above the bolide impact structure, Figure 3.

There are nine aquifer systems in the study area, consisting of one unconfined and eight confined units. The corresponding strata vary in age from Cretaceous to Quaternary. The surficial unconfined Columbia aquifer, confined Tertiary Upper Yorktown-Eastover, Middle Yorktown-Eastover, and a portion of Lower Yorktown-Eastover aquifers contain freshwater. The impact crater is filled with breccia, mixed sediments, other debris, and contains brine water. The approximate position of freshwater Yorktown-Eastover aquifers is also shown in Figure 3.

Figure 4 shows a schematic diagram of nine local, regional aquifer systems and generalized flow lines. The Colombia and the Yorktown-Eastover aquifers contain fresh water. But the other aquifer systems contain saltwater. The Breccia unit (Figure 3) is in the upper Miocene Series and correlates with St. Marys Choptank formation, Powars and Scott (1999). This aquifer and Brightseat aquifer systems contain saltwater; the depth to Upper and Lower Potomac aquifer are about 400 to 530 meters respective-

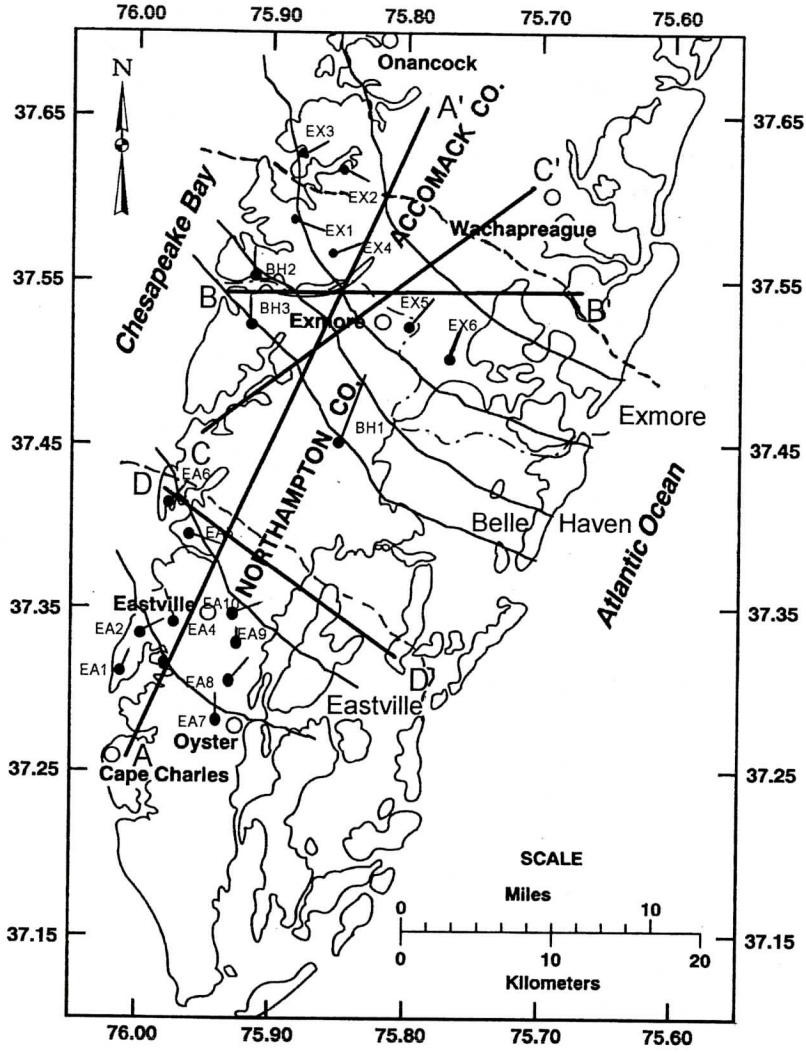

Figure 6. Circles show positions of 25 electric resistivity profiling. The thin-lines connected to circles show the profile's direction. The positions of four resistivity cross sections are shown by thick-lines. Broken lines present the proposed Paleochannel boundaries.

profiles, roads were chosen that crossed the proposed boundaries orthogonally. The a-spacings of 20, 40, 60, and sometimes 80 meters were used to penetrate the Paleochannels at various depths along the profiles. We used the BRGM Syscal R2 receiver and 1000 watts DC transmitter in field operation; A Honda electric generator provided power.

Inversion modeling of field data

The Schlumberger sounding field data were inverted to subsurface geological models with the help of several programs (Zhdanov and Keller 1993 appendix B, Interpex Limited 1999, Zohdy and Bisdorf 1989a and 1989b). The models consisted of horizontal layers with various resistivities and thicknesses. The number of layers should match the local geology. In the upper 100 meters Mixon (1985) recognized up to 12 layers based on a number of boreholes. Richardson (1992) reported nine aquifers and eight confining layers; thus, a total of 17 layers in the upper 700 m is a possibility. Interpex pro-

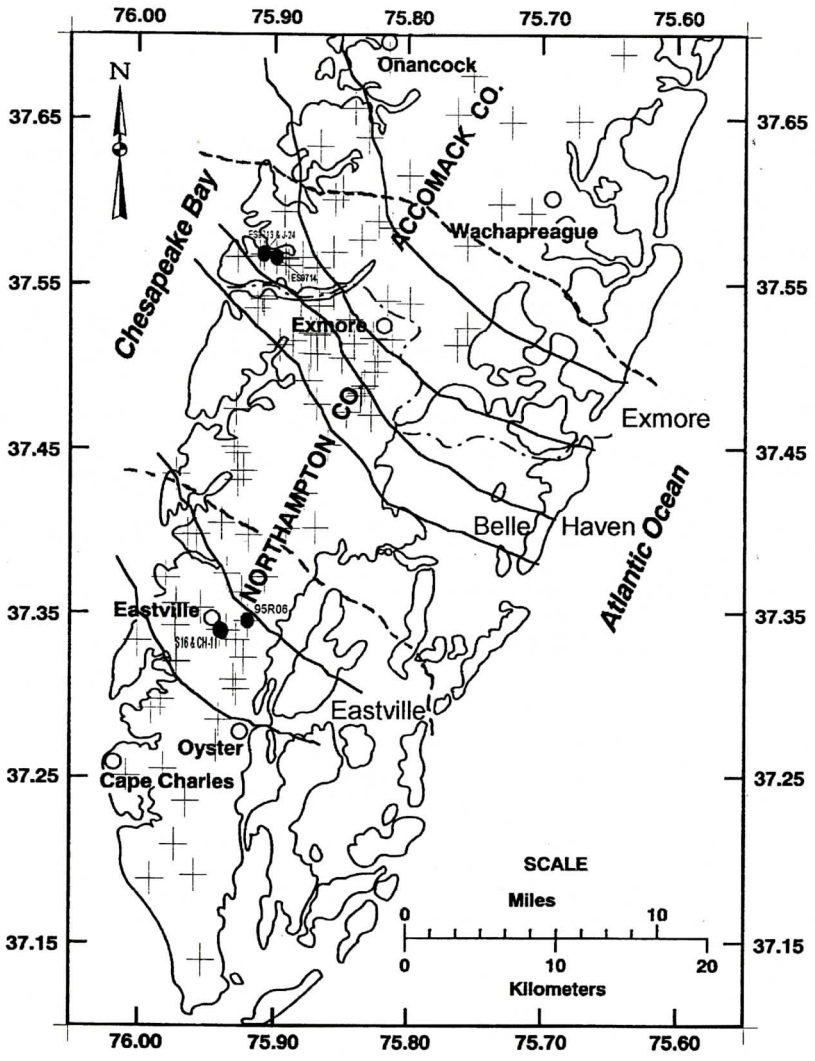

Figure 5. Central locations of 109 electric resistivity soundings are shown by '+' signs. Circles show the central positions of ES9713, ES9714, 95R06 and S16 soundings; the first two are very close to the US Geological Survey boreholes J-24 and the second two are very close to CH-11 respectively. The channel's boundaries are shown by solid lines, and the outer and inner rim of the impact structure are indicated by dashed lines.

segmented. The number of segments depended on the number of times that MN/2 was changed. We had up to three segments. The programs used for inversion of the field curves had options for interpretation of segmented curves. Because we were interested in the deeper depth corresponding to larger AB/2 spacing, we regularly adjusted the field curves for the last segments. The AB/2 spacings were chosen to give the maximum detail and to ensure that the depth of penetration was greater than estimated channel depths of about 60 meters BGS.

In addition, twenty-five Wenner resistivity profiles were conducted across the proposed boundaries of the three Paleochannels. Figure 6 presents locations, approximate lengths, directions of the profiles and the outer and the inner position of the impact structure. Locations of both soundings and profiles were chosen based on availability of suitable straight roads; for

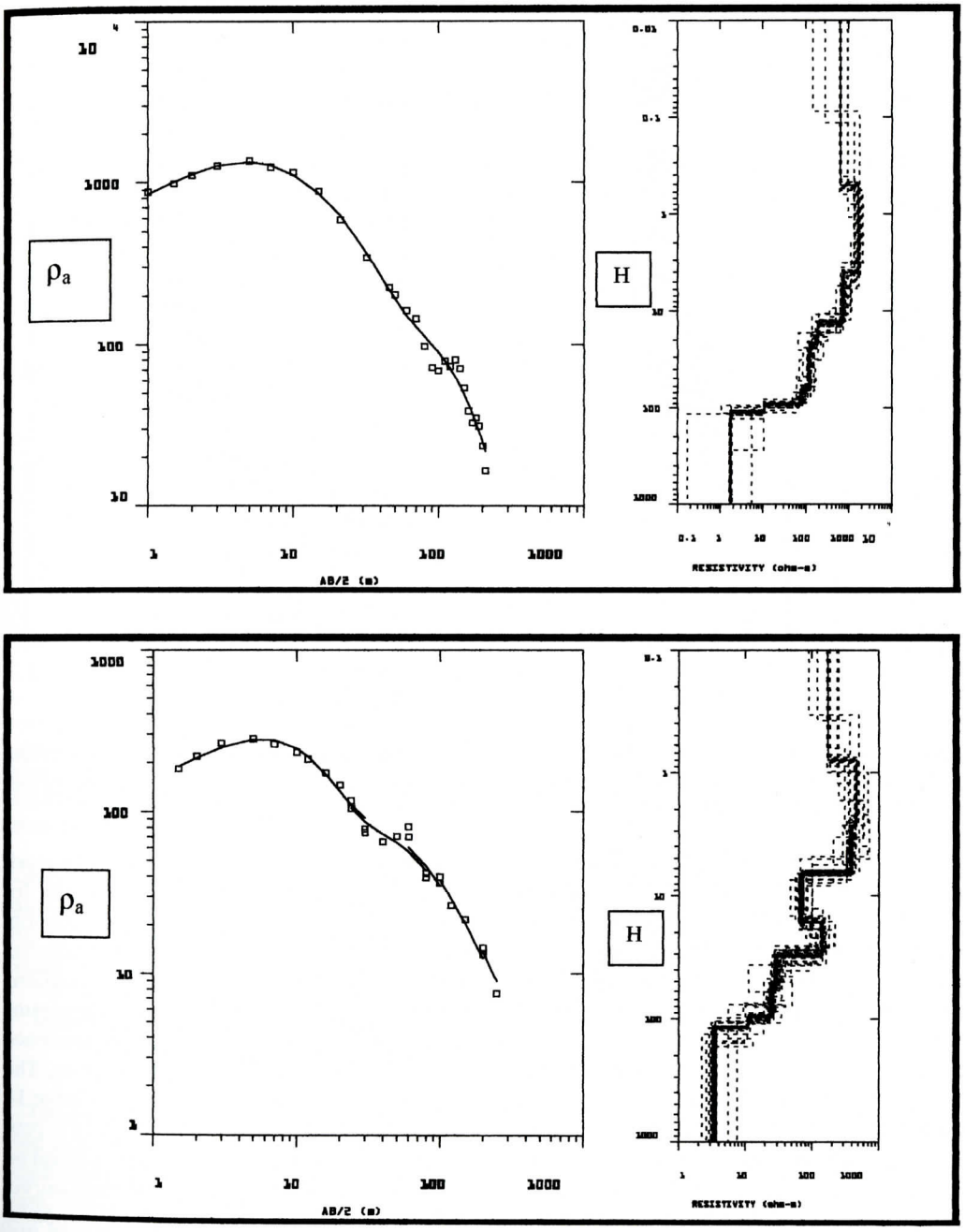

Figure 8. Inversion results for sounding S16 (upper panel) and 97-14 (lower panel). The best-fit model obtained by the Interpex programs produced 10 layers; the equivalence models are also shown on the right. Again, all models produced the same resistivity field curves shown on the left; the three segments of sounding 97-14 are visible, but the segments of sounding s-16 are not shown.

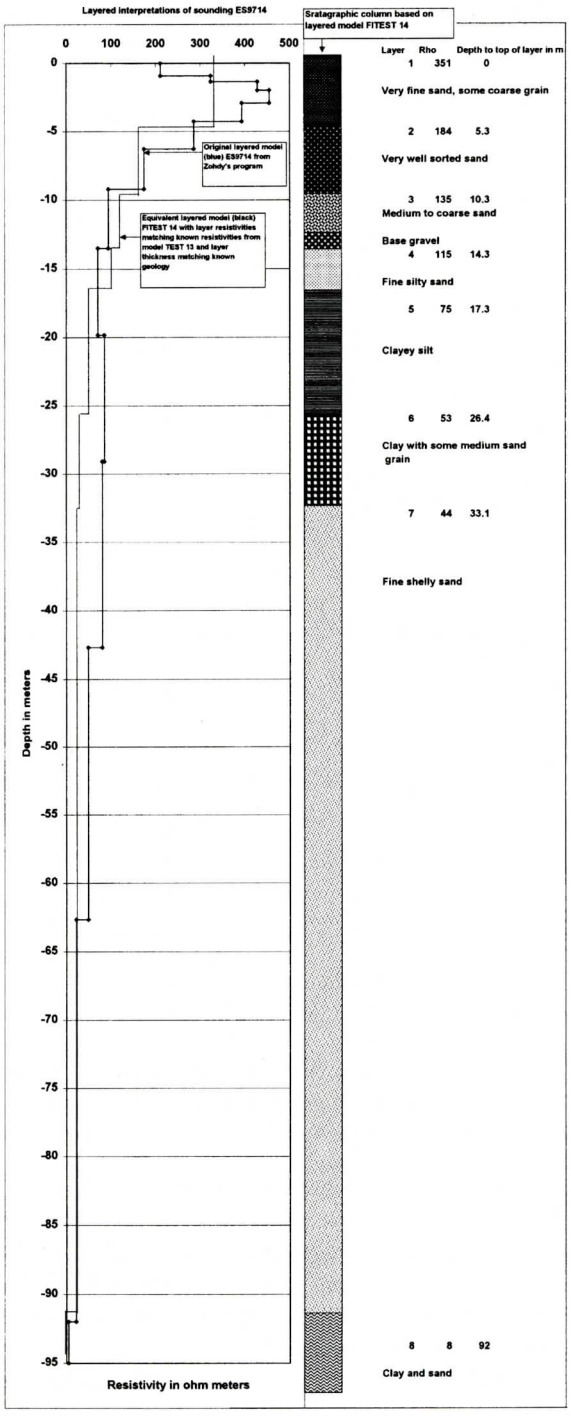

Figure 7. Inversion results for Sounding ES9714. Stratigraphic data are from borehole J-24. The best-fit model produced 15 layers; the borehole data demanded only 10 layers. Both models produce the same resistivity field curves and are equivalent.

grams initially use four layers only. However, local geology demands more units. By using an interactive graphic option the number of layers may be increased to ten. Also, this program allows for interpretation of segmented field curves by shifting the synthetically calculated curve to match the observed field curve. In addition analyses of equivalence may be performed, which allows for a preselected range of errors between the observed and the calculated field curves. The errors may be between five and 15 per cent depending on the quality of the field curves. In the Zohdy and Bisdorf program, the observed segmented field curve is shifted and digitized at six logarithmically equal spacings per cycle. Then the digitized field curve is inverted to obtain the layer thickness and the true resistivity by an iterative method. Finally, when errors between the observed and calculated filed curves are about 2 per cent the results are printed. Although the user may select any number of layers for the model, the program initially assumes that the number of layers is equal to the number of digitized points on the field curve; this is from 14 to 16 in our case. As expected, for a given model, results of inversion for the various programs are nearly the same. However, inversion of a field curve does not produce a unique model; thus, different models may be accepted, simplified or modified to satisfy the known geological information such as borehole data. Model modification is facilitated by application of the equivalence principle (Zohdy, 1989; Burger, 1992; Telford and others, 1976).

In order to ensure that the inversion programs produce geologically reasonable results, soundings ES97 13 and ES9714 were conducted very close to the J-24 borehole and sounding S16 and 95R06 were conducted very close to the CH-11 borehole. Each sounding shows a good match with the respective boreholes. The results for sounding ES97 14

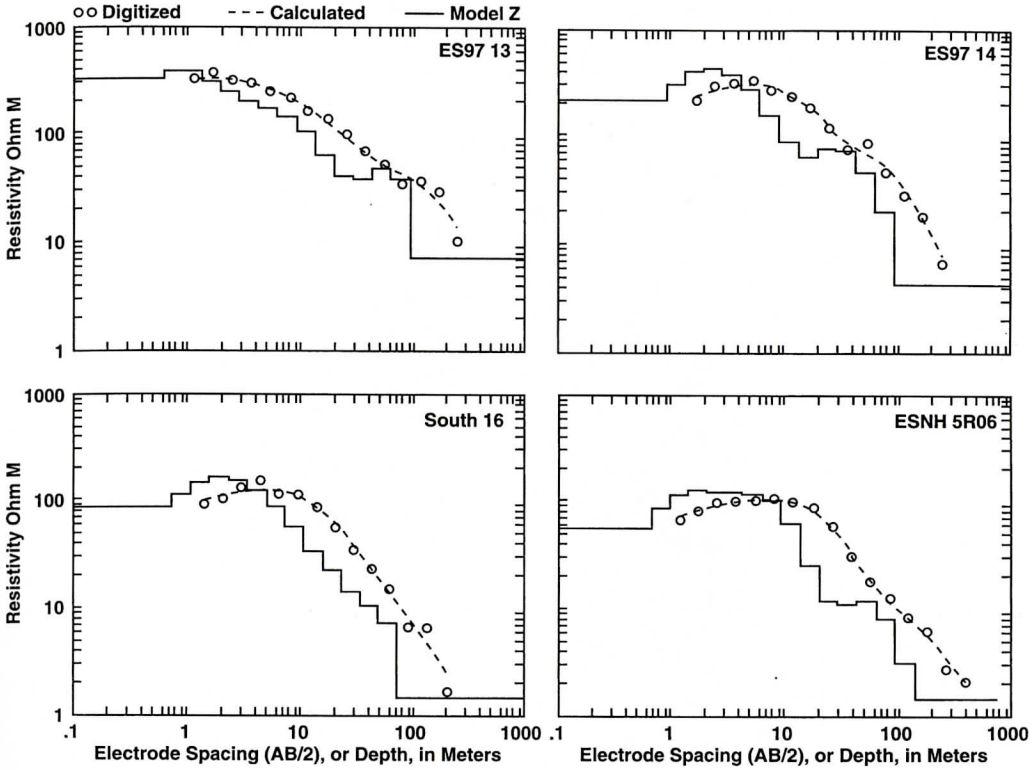

Figure 10. Sounding ES9713, ES9714, S16 and ESNH5R06 are some sample examples from a population of 109 soundings; their locations are shown in Figure 4. Each sounding contains the digitized field curve, circles, the subsurface model-z, solid line, and the theoretical field curve based on model-Z

Zohdy's programs, the results obtained for soundings ES9713, ES9714, South 16 (S16) and ESNH95R06 (95R06), are presented in Figure 10.

Interpretation of Schlumberger resistivity soundings

The inversion results of 109 soundings are used to produce contour maps of resistivity and depth using SURFER software (Golden Software, 1994). The Kriging method of interpolation was used for all contouring to maintain consistency. Contour maps of resistivity are produced at 10 depths: 3, 5, 10, 20, 30, 40, 50, 60, 70, and 100 meters BGS. Channel boundaries are best shown by the 80, 100 and 120 ohm- m contour lines. The areas of higher resistivity within the channel most likely contain high-quality potable water. The 100 ohm-m contours are marked for easy recognition. We marked the 25 ohm-m contours to indicate the position of low resistivity zones with respect to the channel boundaries; these areas indicate poor quality, brackish to salty water. We expect to find that the resistivity contours follow the channel boundaries. Another program was used to calculate depths at preselected mean interval resistivity values for contouring purposes, Zohdy and Bisdorf (1989a, page 61).

We produced both iso-resistivity maps for certain depths and iso-depths maps for certain resistivities. For this study, the 150, 100, 70, 30, 15, 10, 7 and 4.5 ohm-m iso-resistivity surfaces are used. To be brief, we only present resistivity contour maps at depths of 20, 30, 40 and 70 meters, and depth to the 100 ohm-m iso-resistivity surfaces (Figures 11-15). However, we briefly discuss important features of other contour maps. At depths of less than 10 meters,

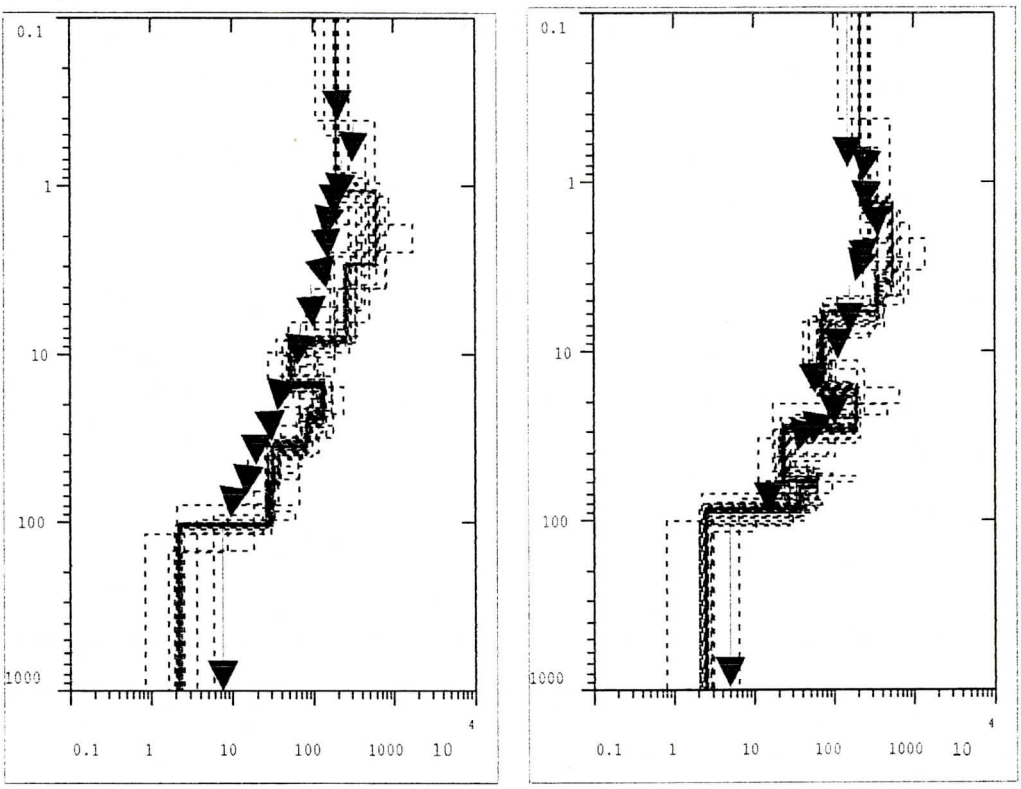

Figure 9. Equivalence 10 layer models for sounding ES9713, and ESNH5R06; the best fitting errors are 7.9 and 12.5 per cent respectively. Models shown by arrows have higher number of layers but a fitting error of 2 per cent.

are presented in Figure 7. The equivalent models that produce the same field curve and satisfy the number of layers encountered by the boreholes are also presented. Our interpretation gives a good approximation of subsurface layering especially at depth higher than about 5 meters.

For brevity, we present only a few examples of our inversion results. The geology of this region demands more than the four layers that the Interpex program initially uses. Thus, we started with a four-layer model, but by interactive interpretation, increased the layers in the model to ten, including the last layer with infinite thickness. This process decreased the fitting error, and the resulting model is closer to geology. Figure 8 presents the inversion results for sounding South 16 and ES97 14 using Interpex 1999 programs. There are ten layers in the model. Fitting errors of the best model are 12.5 and 11.2 % respectively. Figure 9 present the models for ES97 13 and ESNH O95 using both Interpex and Zohdy's programs for comparison. Again, the model for the Interpex programs has ten layers, but the models for Zohdy's programs have 14 layers. The results of Zohdy's programs are not unique, but are within the equivalence models obtained by the Interpex program. The models obtained by Zohdy's programs have 14 layers and smaller errors. The Zohdy's programs start with an initial model that is based on the number of digitized observed field curve, calculates its theoretical curve, and compares the two curves. Then, by an iterative method, depths and resistivities of the initial model are modified until the theoretical curve matches the observed field curve within 2 per cent. When a match is found a plot of the observed field curve, the theoretical field curve and the adopted model are printed. As sample outputs from

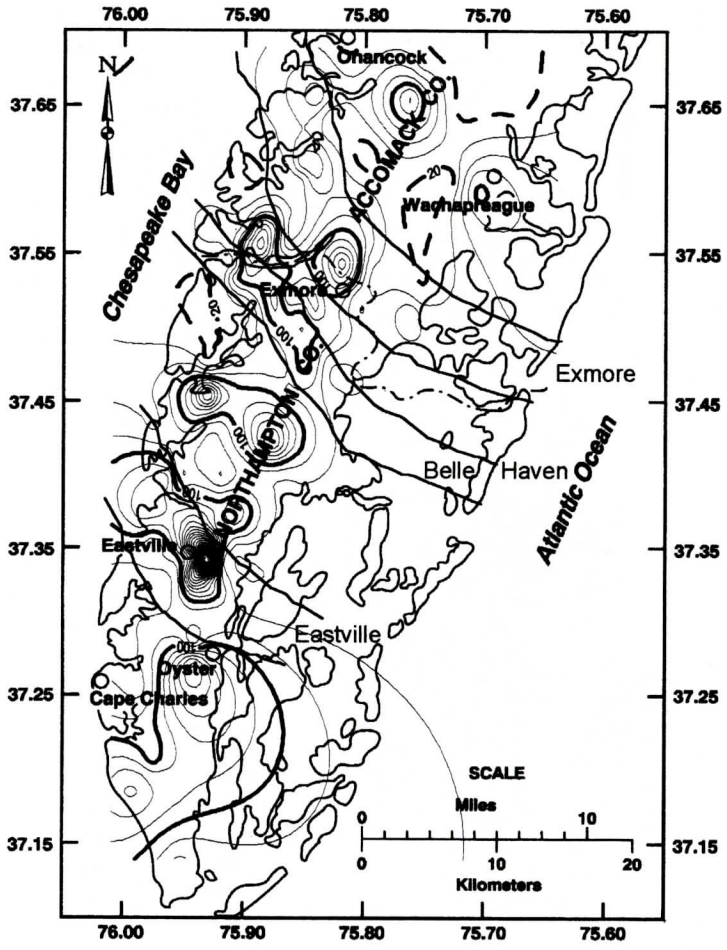

Figure 12. This is the resistivity map at 30 m depth. The 100 ohm-m contours are within the channel boundaries; however, in the case of Eastville and Belle Haven the boundaries are moved slightly toward the north. The contours associated with the Belle Haven channel move toward the boundary of the Exmore Paleochannel. In addition there is one closed 100 ohm-m contour between the two channels. This feature may represent another shallow tributary of the Paleochannels.

three channels. The resistivity features of these maps indicate that the shallower Belle Haven channel is probably a tributary of the deeper Exmore channel. In summary, the trends of both Eastville and Belle Haven channels may be more toward the north near the Chesapeake Bay than previously projected.

Variations of depth to the 150 ohm-m surfaces indicate deepening of the surface along the boundaries of the Eastville and Exmore channels, but variation of depth to the 100 ohm-m surfaces shows deepening of the surface along all three channels' boundaries, Figure 15. This may indicate that Exmore and Eastville contain higher quality water or coarser material than Belle Haven. Figure 15 again indicates that the boundary between the southern part of the Exmore channel and northern part of the Belle Haven channel is merging and these two features are related.

Results of profiles

Several Wenner horizontal profiles are con-

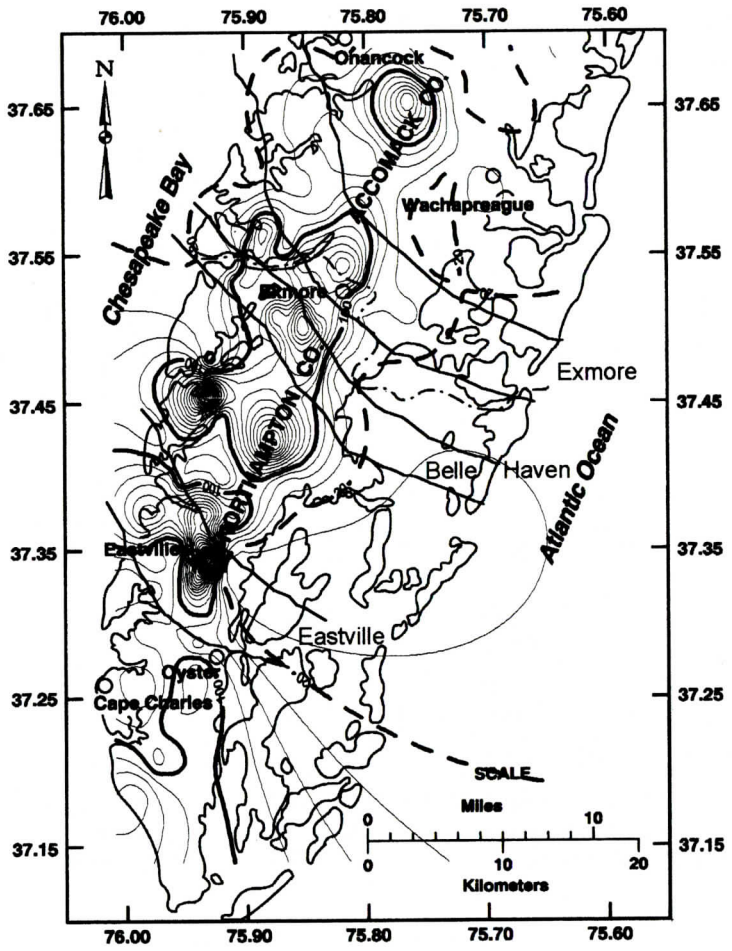

Figure 11. This is the resistivity map at 20 m depth. Contour interval is 25 ohm-m. Heavy lines show the 100 ohm-m contours. Areas with higher resistivity may indicate the effect of channel boundaries at this depth. Within these areas are relatively good quality water. The 25 ohm-m contours are shown by dashed heavy line. Areas with lower resistivity may contain poor quality water.

variations of resistivity contours do not correlate with any of the channel boundaries; thus, the channels are at a greater depth. At shallow depths, high resistivities suggest the coarse sand and gravel of the barrier-spit complex on top of the channel fill sequences. At 20 meters depth, the boundaries of Eastville, Belle Haven, and the Exmore Paleochannels are detected, but the boundaries of the three Paleochannels are nearly merged together, Figure 11. At 30 and 40 meters depth (Figure 12 and 13) the Eastville Paleochannel is observed by higher resistivity contours following its projected boundaries. This map indicates that the channel may extend farther north than previously projected. The southern boundary of Belle Haven and, northern boundary of the Exmore Paleochannel are also visible, but the northern boundary of the Belle Haven Paleochannel appears to be farther north than previously projected; this suggests that the two channels merge. Between 40 and 60 meters depth, resistivity features are similar to the previous maps. At 70 meters depth (Figure 14), only the Exmore channel is well detected which is in agreement with previous statements that the Exmore is the deepest of the

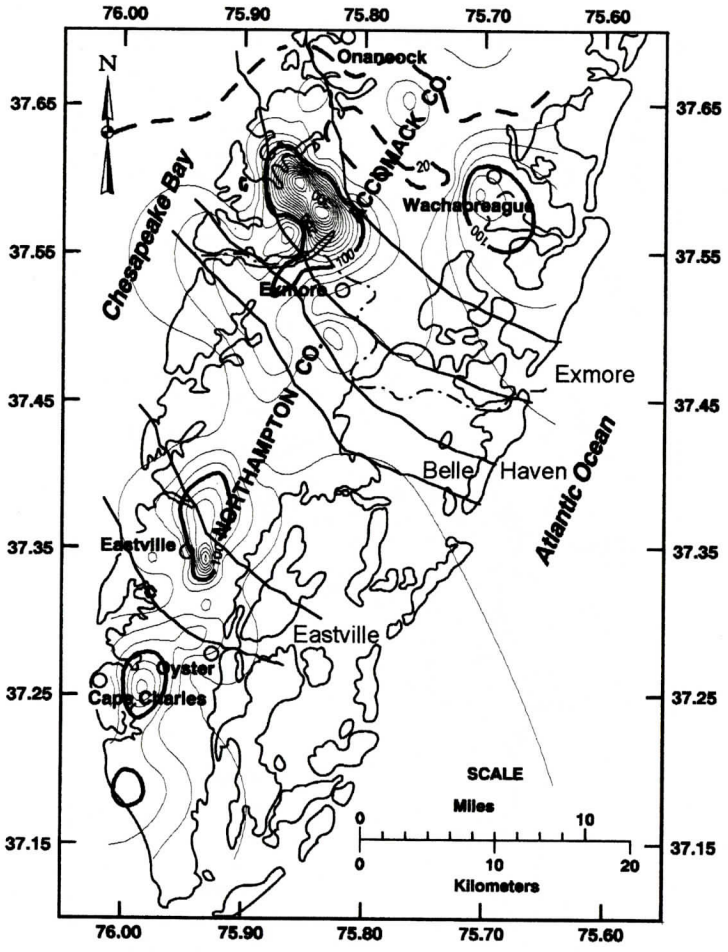

Figure 14. This Figure shows the resistivity map at 70 m depth. The Exmore Paleochannel is still detected, but the Belle Haven Paleochannel is not detected. Thus, the Exmore is deeper than Belle Haven. The contours associated with the Eastville Paleochannel moves further north.

ture is shown on the pseudo-profile EX4 between 600 and 1200 meters and between 200 and 600 meters on profile EX5. Figure 17 presents three profiles (BH1, BH2 and BH3) across the Belle Haven Paleochannel. The proposed boundaries of the channel by Foyle (1994) are also marked. Again, the region with relatively higher apparent resistivity is interpreted as the Paleochannel.

These profiles give evidence that the boundaries of this channel in the area near the Chesapeake Bay are more to the north than previously estimated since BH2 and BH3 do not show a strong apparent resistivity increase across Foyle's estimated boundaries. Pseudo-profiles for this channel did not produce additional information; thus, they are not presented. Profiles EA7, EA8, EA9 and EA10, which are related to the Eastville channel, are presented in Figure 18. Profile EA7 and EA10 cross the boundaries. The southern boundary lies near the 1000 meters mark and is indicated by an increase in apparent-resistivity in this area. The northern boundary lies near the 600 meters mark, again indicated by an increase in apparent resistivity. Profile EA8 and EA9 are within the channel and show variation in the channel's shape. However, the lengths of these profiles are limited; thus, the entire shape of the channel is not sampled.

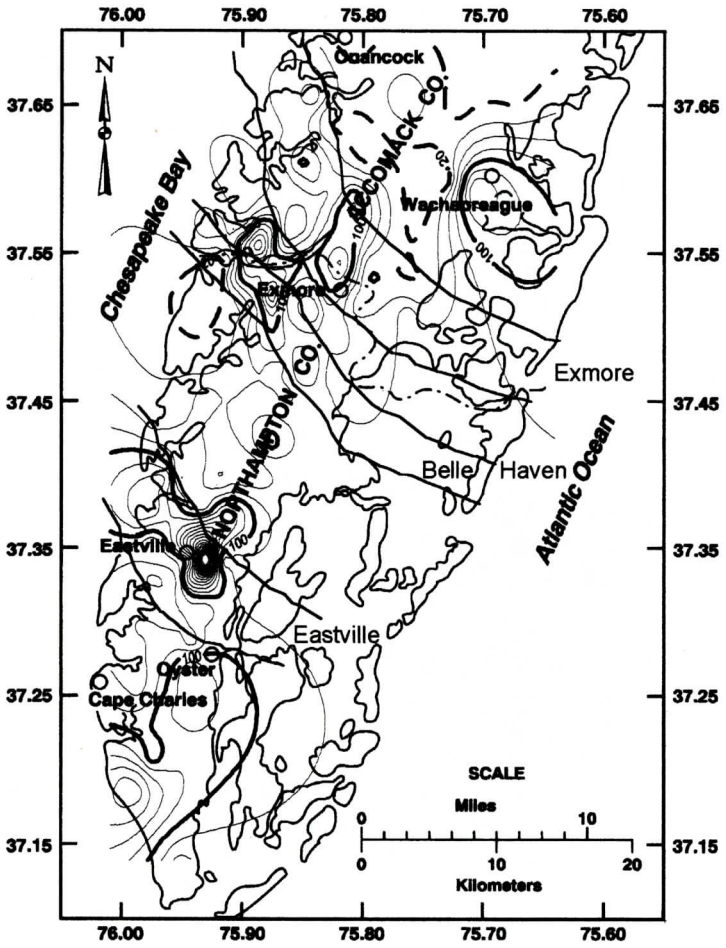

Figure 13. This is the resistivity map at 40 m depth. The 100 ohm-m contours indicate the Paleochannels but are moved toward north.

ducted across and within the estimated boundaries of the Eastville, Belle Haven, and Exmore Paleochannels. Orientation, starting points, and approximate lengths of each profile are presented in Figure 6. Breaks in profiles occur where curves in the road or obstacles such as intersections or bodies of water did not allow equipment to be moved in a straight line. The a-spacings of 20, 40, 60, and sometimes 80 meters were used and gave sufficient depth of penetration to determine if coarser channel fills were being encountered. Plots of apparent-resistivity for each a-spacing versus horizontal distance helped determination of the channels' boundaries. Because these Paleochannels contain higher resistivity material, we expected to see an increase in apparent resistivity for all a-spacings encountering this material when a boundary is crossed. Figure 16 shows profiles EX1, EX2, and EX3, which are associated with the Exmore channel. The upper panels are plots of apparent-resistivity versus distance. The lower panels are pseudo-profiles contoured from these data; they show variation in apparent resistivity with a-spacing instead of depth across a section. Profile Ex1 crosses the southern boundary of the Exmore channel. An increase in apparent resistivity is visible at approximately 800 meters; thus, the boundary may be more toward south and east as shown by the direction of this profile on Figure 6. Profiles EX4 and EX5 are within the channel boundaries; a channel-shaped fea-

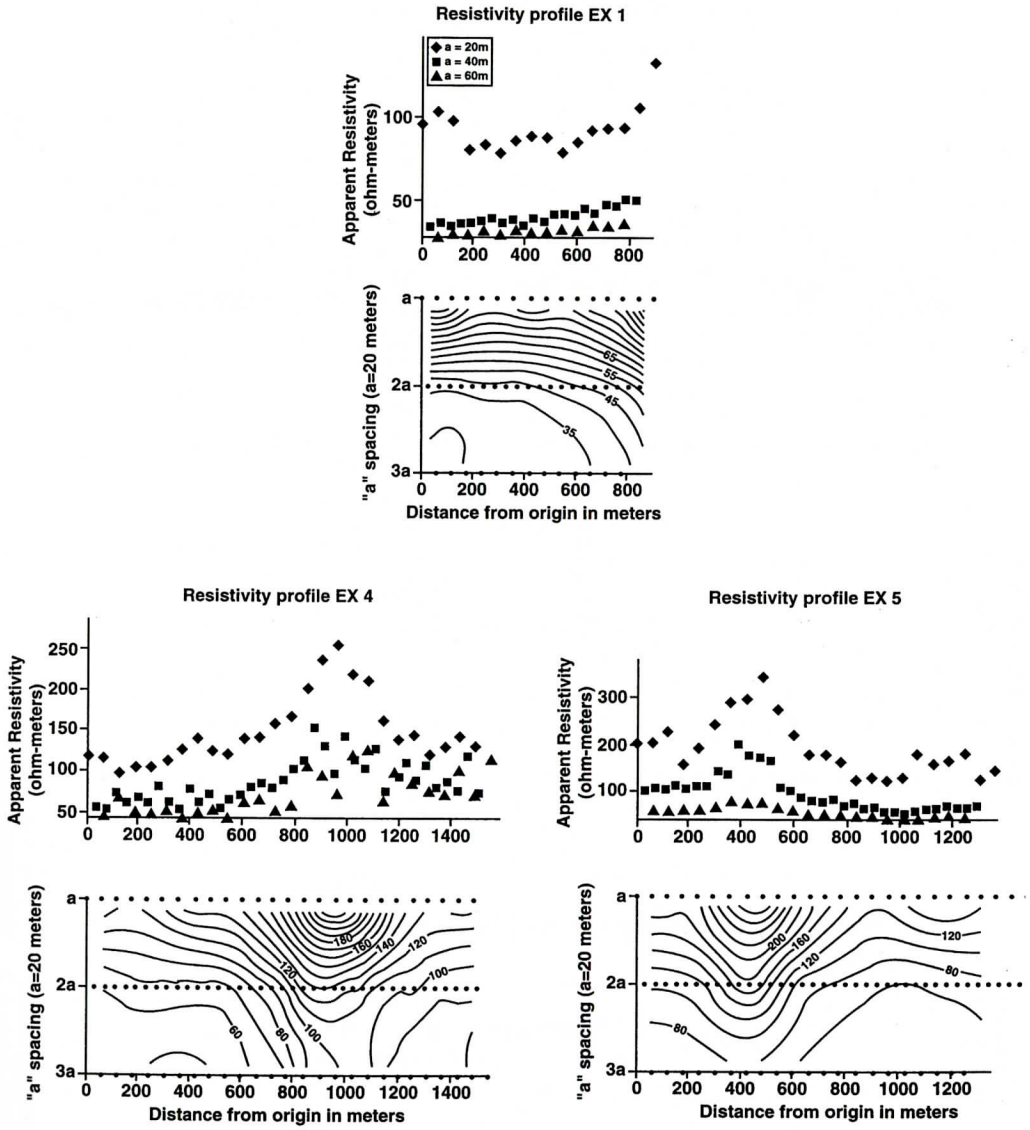

Figure 16. This figure shows three resistivity profiles in the Exmore Paleochannels. For their location and direction refer to figure 5. Profile EX1 crosses the southern boundary. In the upper panel, the increase of apparent resistivity near 800 m marks the channel boundary. Profile EX4 and EX5 are within the channel. They show the increase of apparent resistivity between the 600 m and the 1200 m mark in profile EX4 and between the 200 m and the 600 m mark for profile EX5. The lower panels show the pseudo-profiles. The apparent channel-like features are detected by deepening of high resistivity contours.

meters BGS along cross section CC'. Furthermore, the depth of the Belle Haven Paleochannel along BB' is about 40 meters BGS which is in good agreement with Foyle's estimates. BB' and CC' show the southern boundary of the Exmore and the northern boundary of the Belle Heaven Paleochannels merging; thinner lines show the merged boundaries. Cross section DD' shows the shape of Eastville channel along its most northern boundary; along this cross sec-

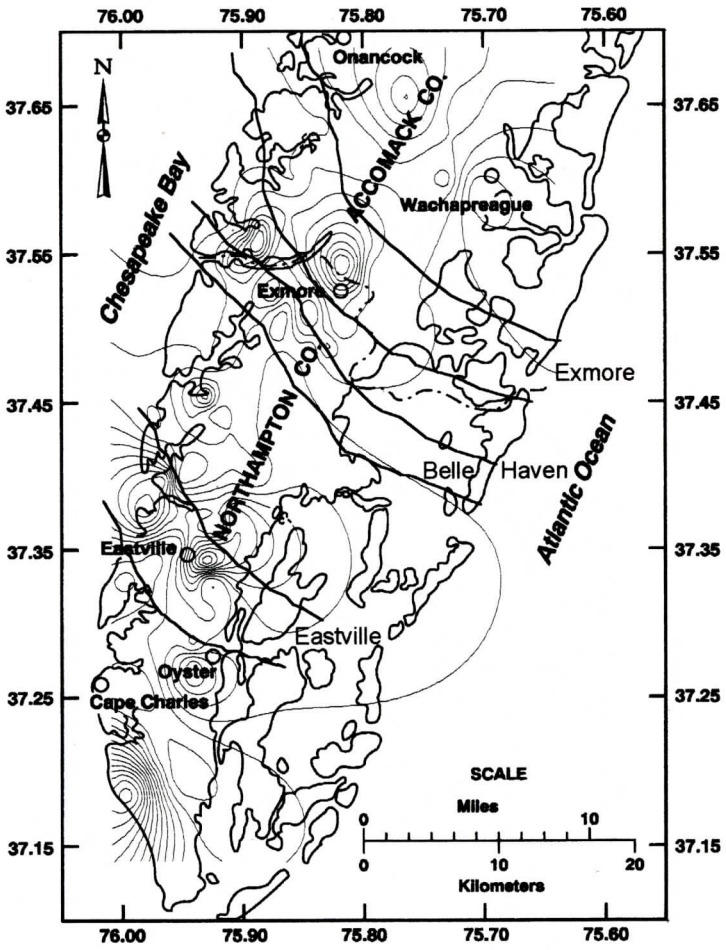

Figure 15. This Figure shows the depths to the 100 ohm-m iso-resistivity surface. The surface is deepening within all channels; however, for the Exmore Paleochannel maximum depth is within the channel boundaries, but for others this feature is moved toward the north.

Interpretation of cross sections

Four resistivity cross-sections, AA', BB', CC' and DD' are constructed using the ten resistivity contour maps discussed before. Cross sections are presented in Figure 19. Their lengths are 48, 24, 27 and 19 km respectively. The previously proposed surface boundaries and the names of the channels are also marked. Heavy lines mark the 80, 100 and 120 ohm-m contours; they appear to be guides for variations in the channels' boundaries with respect to depth.

Cross section AA' crosses all three Paleochannels. Mixon (1985) gives a maximum depth of about 60 meters below sea level or about 70 meters BGS for the Eastville Paleochannel. Assuming that the 100 ohm-m is an average representation of the channel fill, we note that the resistivity cross sections also give a maximum depth of about 70 meters BGS for this Paleochannel. Cross sections AA' and BB' show that there is no distinct boundary between the Exmore and Belle Haven Paleochannels. The Belle Haven channel appears to be a shallower tributary of the Exmore channel on this cross section.

The 100 ohm-m contours show a maximum depth of about 90 meters BGS for the Exmore Paleochannel along cross section AA', 80 meters BGS along cross section BB', and 60

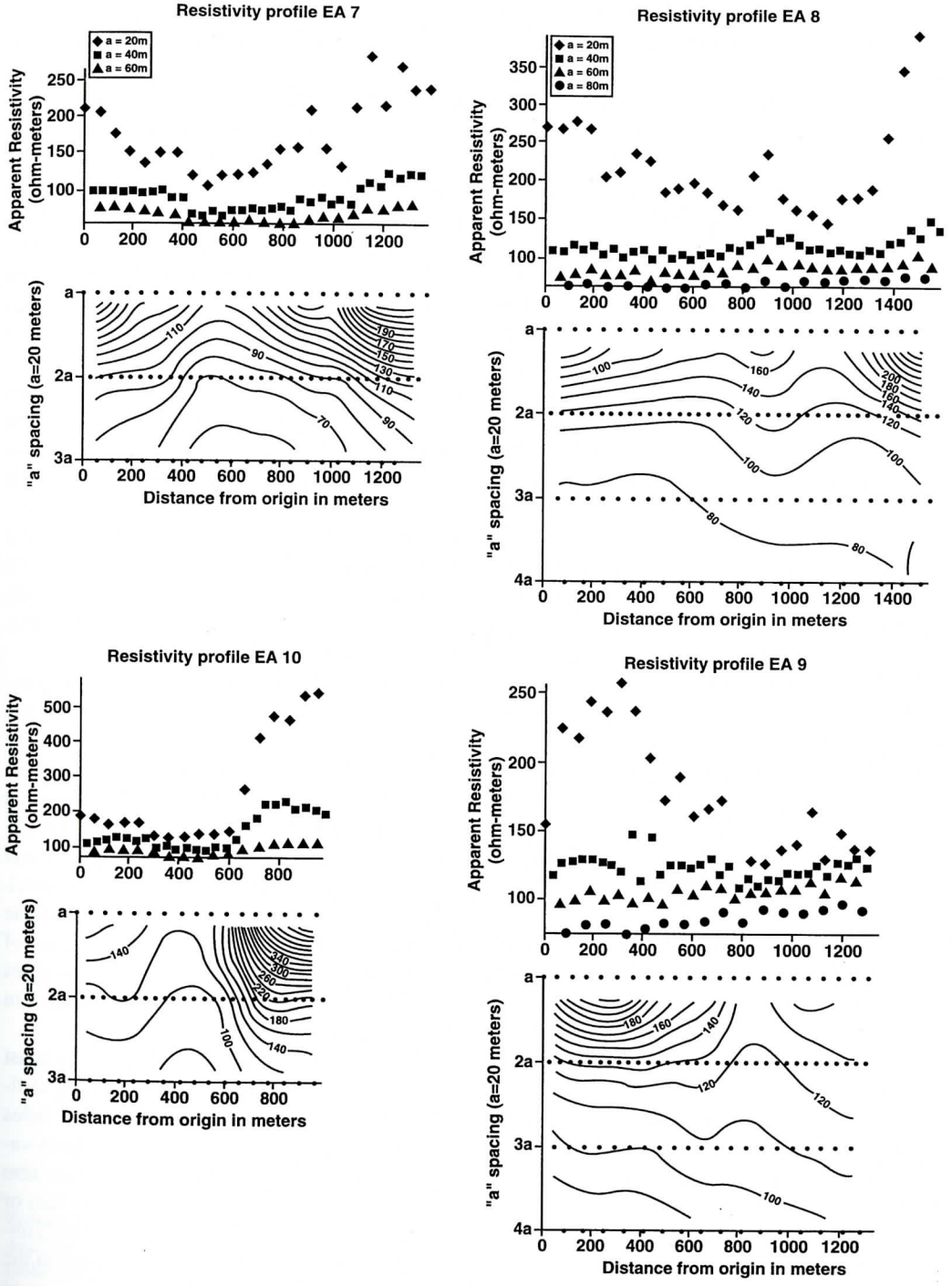

Figure 18. This figure shows four resistivity profiles in the Eastville Paleochannel. Profile EA7 and EA10 cross the boundary; profile EA8 and EA9 are within the Paleochannel. On profile EA7 boundary starts about 1100 m mark; on profile EA10 boundary is about 600 m mark. Profile EA8 and EA9 are within the Paleochannel. The deepening of the high apparent resistivity contours on the pseudo-profile shows Paleochannels.

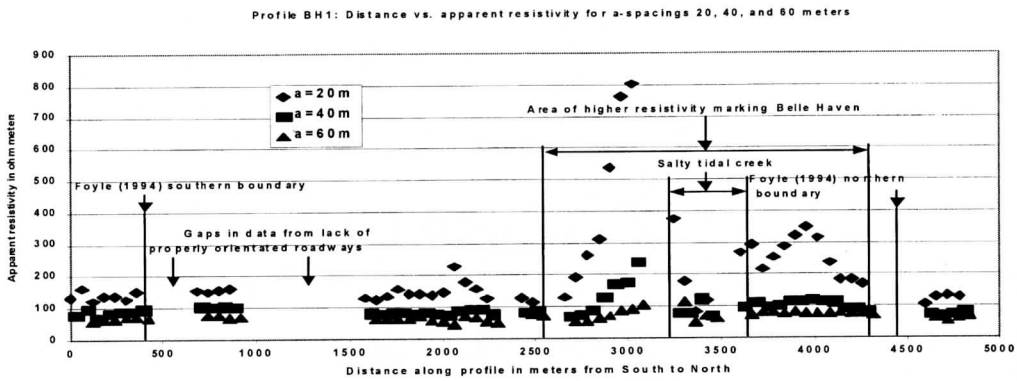

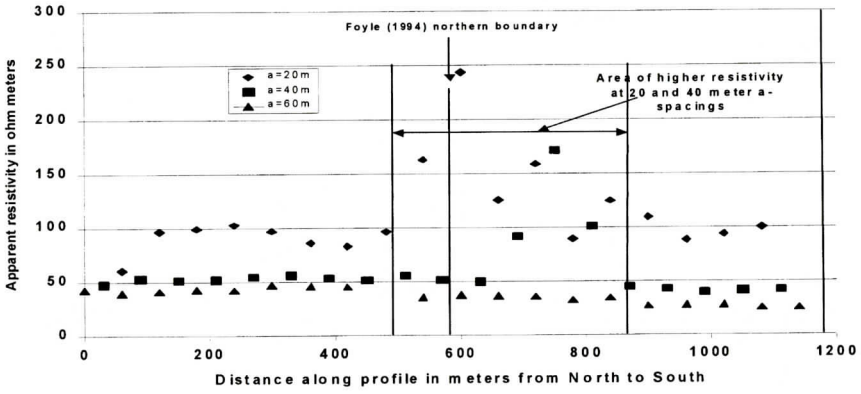

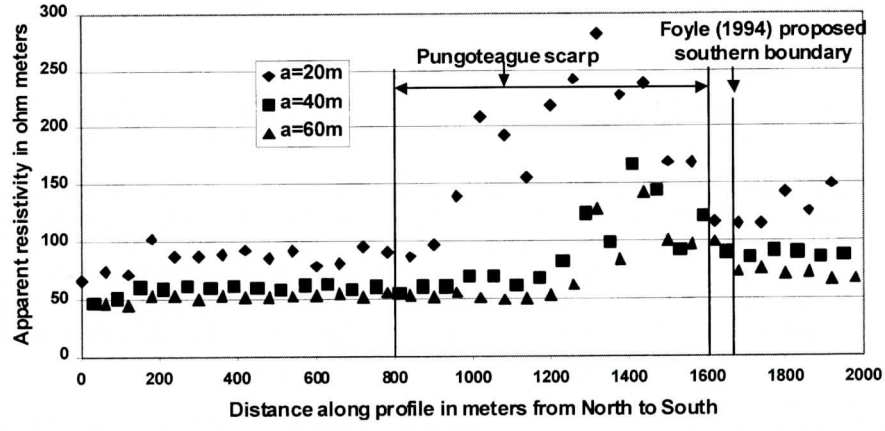

Figure 17. This figure shows three resistivity profiles in the Belle Haven Paleochannel. A region of high apparent resistivity marks the position of boundaries. The southern boundary appears north of the suggested boundary by Foyle (1994).

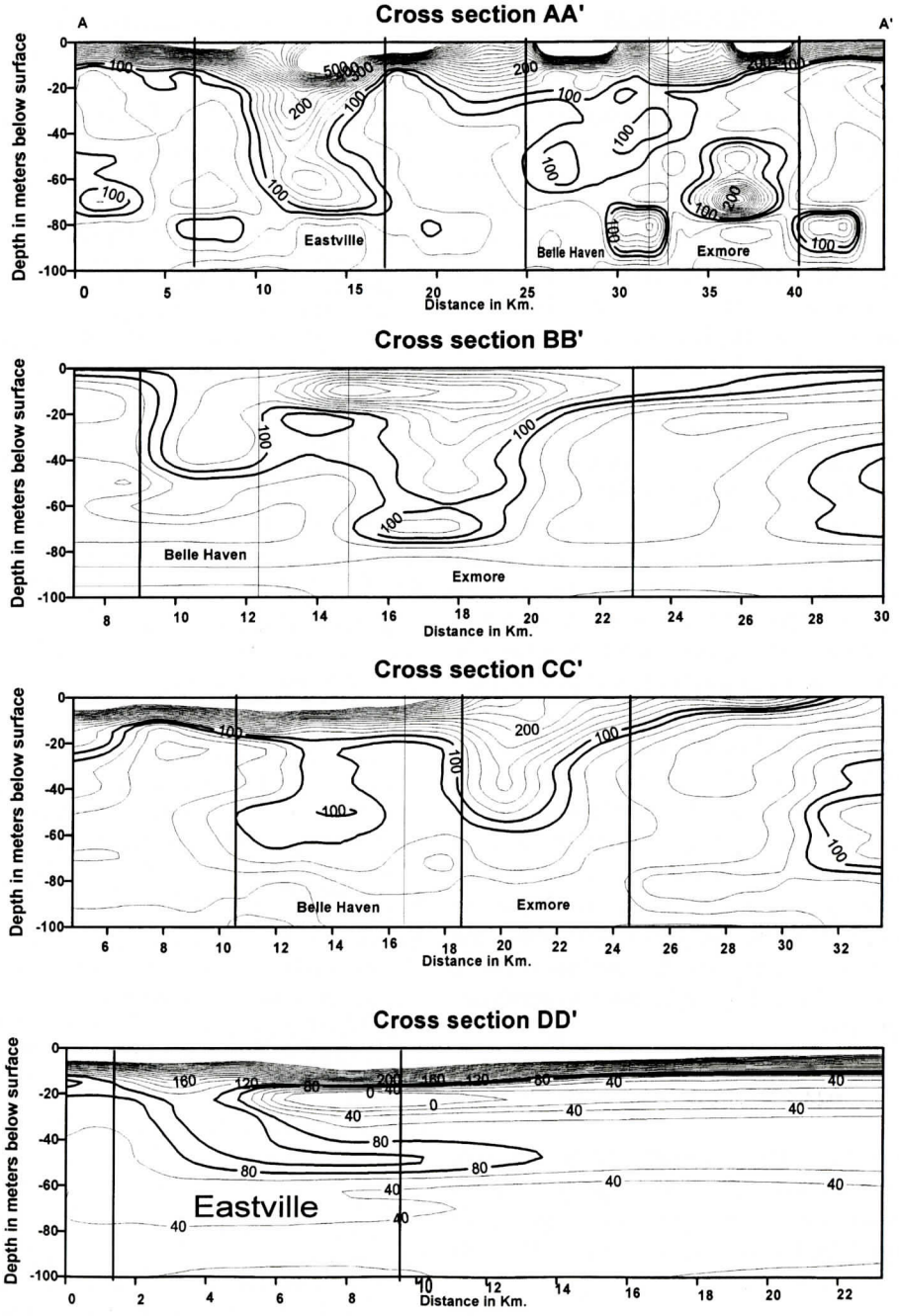

Figure 19. This figure shows the four resistivities cross-sections across the Paleochannels. For section construction true resistivity maps at 10 different depths are used; refer to text please. Solid heavy lines show the 80 and 100 ohm-m contours. Various channel boundaries are marked. The areas with higher resistivity are interpreted as Paleochannels' fills. They contain relatively high quality water. The dashed heavy lines show contour with resistivities of less than 20 ohm-m. These regions contain low quality brackish water. Cross section AA', BB' and CC' suggest that Belle Haven is a tributary of the Exmore Paleochannel; their adjacent boundaries are shown by thin lines. The Eastville Paleochannel appears to extend further north.

tion its depth is about 50 meters BGS. This profile indicates that the boundary in this area may extend further north.

Resistivity decreases in areas near the coastline of the Bay and Atlantic Ocean. These trends are caused by a combination of regional hydrogeology and geology. The unsaturated soil horizon had higher resistivities than the finer grained and saturated Tertiary deposits. The water table within the Columbia aquifer is shallower near the Bay and ocean, causing surficial resistivity values to decrease in these areas. Quaternary sediments in the Eastern Shore also are thinner toward the Bay and ocean (Mixon, 1985). That is also shown by the lower resistivity values. Intrusion of saltwater into Quaternary sediments also causes resistivity values to decrease near coastal areas (Nowroozi et al. 1999).

The base of the Chesapeake impact structure is about 2 km below the surface and the diameter of its outer rim is about 90 km wide. The impact craters, which contain saltwater, are well below the 100 meters depth and 20 ohm-m contours shown in Figure 19. The Exmore and Belle Haven Paleochannels are between the inner and outer rim of impact structure, whereas the Eastville Paleochannel is within the inner rim.

DISCUSSION

The Exmore, Belle Haven, and Eastville Paleochannels are detected by their resistivity contrast between the channel fill and surroundings sediments. The contrast is associated with both the coarser-grained channel fill and high-quality fresh ground water in the channels. Analysis of the resistivity data indicates that Belle Haven is 40 to 60 meters BGS and, it is merging with and/or associated with the Exmore near the coast of the Chesapeake Bay. Its width is approximately 4 km but varies across it length. Cross section AA' is nearly orthogonal to the proposed channels' boundaries. This cross-section indicates that the Belle Haven Paleochannel may be a shallower tributary of the deeper Exmore channel. The Eastville and Exmore channels show up strongly as areas of increasing resistivity at depths in agreement with previous estimates with resistivity contour lines following channel-like shapes. Furthermore, the high resistivity contour trend of the Eastville channel extends outside its estimated northern boundary. Cross-section CC' was chosen such that its direction is orthogonal to the projected boundaries of the Exmore and Belle Haven Paleochannels. Cross section BB' cuts the proposed boundaries at an acute angle. As can be seen from cross section BB' and CC', Belle Haven shows up as a channel-like feature of high resistivity close to Exmore. These cross-sections also show Belle Haven (40 to 60 meters BGS) to be shallower than Exmore (70 meters BGS), which is in good agreement with Foyle (1994). Cross-section DD' crosses the Eastville Paleochannel near its most northern boundary and shows a channel-like feature with a depth of 50 meters BGS; this depth is based on the 100 ohm-m contour. However, the maximum depth of this Paleochannel is approximately 70 meters BGS as indicated in cross section AA'.

The Wenner profile data gives supporting evidence that Belle Haven does not follow the track previously proposed by Foyle (1994). The eastern profile, BH1, shows a high apparent resistivity trend approximately 2 km wide with a pseudo-depth reaching 60 meters BGS. We believe this trend is the result of coarser sand and gravel within the Belle Haven Paleochannel. The western profiles, BH2 and BH3, cross the estimated boundaries but show no signs of coarse material along their transects. This gives more evidence that the estimated boundaries in this area are incorrect.

There are low resistivity zones near the coast and below the channel boundaries. They indicate saltwater percolation by storms or tides near the coast, or over exploitation of freshwater from the channels. The channels may also transport freshwater into the Chesapeake Bay or Atlantic Ocean; Manheim and others (2002) observed submarine freshwater discharging on the western margin of the Chincoteague Bay at depth of less than 40 meters. The base of the Chesapeake impact structure is about 2 km below the surface and its upper features occur below the 100 meters depth shown in Figure 19.

squares method. Geophysics, 47,2, 244-256.

Nowroozi, A.A., Horrocks, S.B., and Henderson, P.N., 1999. Saltwater intrusion into the freshwater aquifer in the Eastern Shore of Virginia: A reconnaissance electrical resistivity survey. In press. Journal of Applied Geophysics.

Poag, C.W., 1996. Structural outer rim of Chesapeake Bay impact crater: Seismic and borehole evidence. Meteoritics & Planetary Sciences 31,218-226.

Poag, C.W., 1997. The Chesapeake bolide impact: a convulsive event in Atlantic coastal plain evolution. Sedimentary Geology,108, 45-90.

Poag, C.W. 2002. USGS, Science for a changing world. Ancient Cataclysm. Http://woodshole.er.usgs.gov/epubs/bolide/.

Powars, D.S.,2000. The effects of the Chesapeake Bay impact crater on the Geological framework and the correlation of hydrogeologic units of southeastern Virginia, South of the James River. USGS, Professional Paper 1622.

Powars, D.S. and Scott T. B.,1999. The effect of the Chesapeake Bay impact crater on geological framework and correlation of hydrogeologic units of the lower York-James Peninsula, Virginia. USGS Professional Paper 1612.

Richardson, D.L. 1992. Hydrogeology and Analysis of the Ground-Water Flow System of the Eastern Shore, Virginia. U.S.G.S. Open-file report 91-490, 119 pp.

Telford, W.M, Geldart, L.P., Sheriff, R.E., and Keys, D.A., 1976. Applied Geophysics. Cambridge University Press.

Ward, S.H., 1990. Geotechnical and Environmental Geophysics volume 1: review and tutorial. Society of Exploration Geophysicists, p. 147-189.

Zhdanov, M.S. and Keller, G.V., 1994. The Geoelectric Methods in Geophysical Exploration: Methods in Geochemistry and Geophysics Volume 31. Elsevier Science B.V. Netherlands.

Zohdy, A.A.R., Eaton, G.P., and Maybey, D.R., 1974. Application of surface geophysics to Groundwater investigations: Techniques of Water-Resources Investigation of the United States Geological Survey, Book 2, Chapter D1, 116 pp.

Zohdy, A.A.R., 1989. A new method for the automatic interpretation of Schlumberger and Wenner sounding curves. Geophysics, 54: 245-253.

Zohdy, A.A.R., and Bisdorf, R.J., 1989. Programs for the Automatic Processing and Interpretation of Schlumberger Sounding Curves in Quickbasic 4.0. USGS Open-File Report 89-137 A.

CONCLUSIONS

We used electrical resistivity to detect and better delineate the onshore tracts of three Paleochannels beneath the Eastern Shore of Virginia. Resistivity differences between coarser channel-fills (sand and gravel) and surrounding finer grained material (fine silt and sand) provide sufficient resistivity contrast to allow these channels to be imaged electrically. Based on the resistivity data, the land tracts of the Exmore and Eastville Paleochannels are nearly the same as previously estimated with the exception of the Eastville's northern boundary extending slightly more to the north. However, our data suggests the onshore tract of Belle Haven follows a slightly different path than previously proposed by Foyle (1994) and is related to the Exmore. Our data suggest that relatively high-quality water may exist within the channels and that relatively poor-quality brackish water lies at depths of more than 80 meters BGS under the channels. Furthermore, in coastal area outside the channel boundaries, brackish water may be at depths as shallow as 20 meters BGS. This may be occurring because of over-pumping of wells within the highly permeable channel-fill or direct percolation during storms or high tides. The impact structure containing brine water is between 300 and 500 meters under the lower part of Chesapeake Bay and surrounding peninsulas. Thus, it is under our maximum observed depth.

ACKNOWLEDGMENTS

This research was supported in part by grant 552131, VA Tech CR-4963 from the Virginia Water Resources Research Center, and Grant 752911 VCI Eastern Shore from the Virginia Coast Institute.

REFERENCES

Burger, H.R., 1992. Exploration Geophysics of the Shallow Subsurface, Prentice Hall, Inc. NJ.

Colman, S.M. and Mixon, R.B. 1988. The Record of Major Quaternary Sea-level Changes in a Large Coastal Plain Estuary, Chesapeake Bay, Eastern United States. Palaeogeogr.

Colman, S.M., Halka, J.P, Hobbs, C.H. III, Mixon, R.B., and Foster, D.S. 1990. Ancient Channels of the Susquehanna River beneath Chesapeake Bay and the Delmarva Peninsula. GSA Bulletin, 102: 1268-1279.

Darwin, R.L. 1988. Geoelectric stratigraphy and subsurface evaluation of Quaternary deposits of copper Basin, Northeast Texas. University of Texas, Arlington, Master's degree Thesis, 140 pp.

Donohue, D.A. 1989. Paleochannel aquifer potential at Montana State University; a test of hypotheses. Montana State University, Master's degree Thesis, 94 pp.

El-Gamili, M.M., Shaaban, F.F., and El-Morsi, O.A., 1994. Electrical resistivity mapping of the buried stream channel of the Canopic branch of the western Nile Delta, Egypt. Journal of African Earth Sciences, 19: 135-148.

Foyle, A.M. 1994. Quaternary Seismic Stratigraphy of the Inner Shelf Coastal Zone, Southern Delmarva Peninsula, Virginia. Department of Oceanography, Old Dominion University, Ph.D. Thesis. 467 pp.

Foyle, A.M. and Oertel, G.F., 1992. Seismic Stratigraphy and Coastal Drainage Patterns in the Quaternary section of the Southern Delmarva Peninsula, Virginia, USA. Sedimentary Geology, 80: 261-277.

Golden Software, 1994. Surfer for Windows: Contouring and Mapping. Golden, CO.

Hansen, H. J. III. 1966. Pleistocene Stratigraphy of the Salisbury Area, Maryland, and its Relation to the Lower Eastern Shore-A Subsurface Approach. Maryland Geological Survey Report of Investigations, **2**, 56 pp.

Harrison, S.C. 1972. The sediments and sedimentary processes of the Holocene tidal flat complex, Delmarva Peninsula, Virginia. Baton Rouge, Louisiana, Louisiana State University Coastal Studies Institute Technical Report 112, 107 pp.

Harrison, W., Malloy, R.J., Rusnak, G.A., and Terasmae, J., 1965. Possible late Pleistocene uplift, Chesapeake Bay entrances. Journal of Geology, 73: 201-229.

Interpex Limited, 1999. RESIX-IP Volume 2, User's manual DC resistivity and induced Polarization Data interpretation Software P.O. Box 839 Golden Colorado 80402-0839.

Johnson, G.H, Kruse, S.E., Vaughn A.W., Lucey, J.K., Hobbs III, c.h. and Powars, D.S. (1998). Postimpact deformation associated with the late Eocene Chesapeake Bay impact structure in southeastern Virginia. Geology 26 507-510.

Manheim, F.T., Krantz, D.E. Snyder, D.S. and Sturgis, B., 2002. Streamer resistivity survey in Delmarva Coastal Bays. Proceeding Symposium on Application of Geophysics to Environmental and Engineering Problems (SAGEEP) paper 136 SL5, 17 p.

Mixon, R.B., 1985. Stratigraphic and geomorphic framework of uppermost Cenozoic deposits in the southern Delmarva Peninsula, Virginia and Maryland. U.S. Geological Survey Professional Paper 1067-G, 53 pp.

Murakami, N., and Uchida, S. (1982). Accuracy of the filter coefficients determined by the iteration of the least

SOUTHEASTERN GEOLOGY
V. 41, No. 4, March 2003, p. 201-223

THE CRABTREE PEGMATITE, SPRUCE PINE DISTRICT, NORTH CAROLINA: MINERALIZATION AND HOST ROCK RELATIONSHIPS

CHRISTINE M. TAPPEN[1]

MICHAEL S. SMITH

Department of Earth Sciences, University of North Carolina at Wilmington, Wilmington, North Carolina 28403

1. Department of Earth and Planetary Sciences, American Museum of Natural History, Central Park West @ 79th St., New York, New York 10024-5192.

ABSTRACT

The Crabtree pegmatite in the Spruce Pine District of North Carolina is an albite-rich beryl (emerald, green, aquamarine and yellow) and tourmaline-bearing granitic pegmatite. Although it is texturally unzoned, the pegmatite is weakly differentiated with slightly coarser grained segregations and aplitic units. Locally, the pegmatite contains variously assimilated biotite schist xenoliths. The host rocks for the pegmatite include quartz-mica schist at the western pegmatite contact and chlorite schist at the eastern contact. Chlorite schist and biotite schist alteration aureoles or zones are associated with pegmatite intrusion. Emerald with subordinate green beryl mineralization occurs mainly in alteration haloes and less frequently in the pegmatite margin. Yellow beryl occurs in the margin, center of the pegmatite, and near the biotite schist xenoliths. Rare aquamarine occurs in the pegmatite as well. Tourmaline occurs in the exocontacts, the pegmatite margin and in the biotite schist xenoliths.

The Crabtree emerald in the biotite and chlorite schist exocontacts has higher Na_2O, Cs, Rb, FeO (tot), MgO, Cr, Ni and V concentrations than the yellow beryl and aquamarine in the pegmatite. Alkali enrichment in the Crabtree emerald suggests it formed at the final stage of beryl mineralization. The tourmaline chemistry is between dravite and schorl compositions. Crabtree tourmaline has elevated F concentrations with values reaching 0.8 apfu in the exocontacts and the pegmatite margin. High alkali and F enrichment indicate that fluid transport rather than fractionation is the cause for rare element distributions. Cr tends to occur in higher concentrations in Crabtree tourmaline of the exocontacts, especially the chlorite schist exocontact, where it reaches values of 0.14 apfu. At the Crabtree deposit, intrusion of a sodic magma into originally mafic schist resulted in interaction and migration of Cr from the chlorite schist into the pegmatite to produce emerald during contact and regional metamorphism.

INTRODUCTION

In the United States, one of the commonly reported locations for gem quality emerald is the eastern Blue Ridge Belt of North Carolina. Although several thousand pegmatites are exposed in the Spruce Pine mining district of the eastern Blue Ridge Belt, only 28 reported mined pegmatites contain beryl (Lesure, 1968; Wiener and Merschat, 1990). The Crabtree pegmatite has been sporadically mined for gem-quality beryl since 1894. It has produced a number of good quality emeralds, one of which was 70 carats (Sinkankas, 1981). Despite the notoriety of this pegmatite, no detailed geological, petrological, or geochemical investigation of it has ever been published and very little geologic or geochemical information has been reported for the host rocks, pegmatite, or beryl and tourmaline mineralization (Furbish, 1972; Broughton, 1974; Sinkankas, 1981; Kazmi and Snee, 1989). The purpose of this paper is to pro-

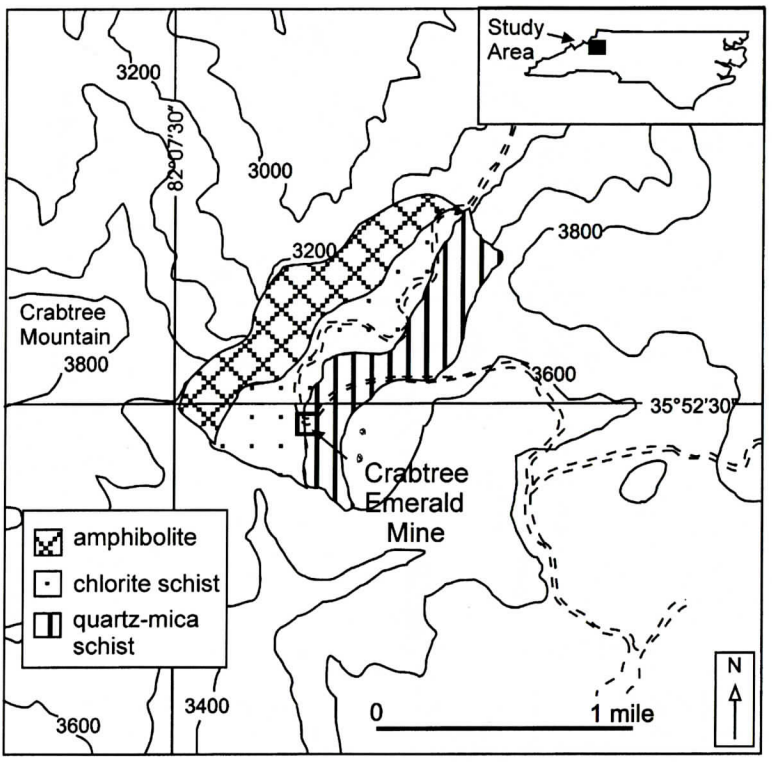

Figure 2. Reconnaissance geology of the Crabtree pegmatite and surrounding host rocks on a USGS topographic base map.

schists and gneisses (Raymond, 1998). Ultramafic and mafic rocks such as meta-dunites and chlorite schists are widely distributed but less significant volumetrically. The overlying Alligator Back Metamorphic Suite is comprised of metapelites and metasandstones (Abbott and Raymond, 1984).

Acadian-age plutons and associated granitoid pegmatites cut the Ashe and the Alligator Back metamorphic suites. Rb-Sr whole-rock age dates on two pegmatites are 404 ± 14 and 392 ± 15 m.y. according to Kish (1989) whereas Johnson et al. (2001) determine U-Pb dates derived from zircons as 377± 2.5 m.y. The granitoid pegmatites exclusively intrude kyanite facies and higher-grade metamorphic rocks, indicating that emplacement occurred during middle amphibolite facies and higher-grade metamorphic events (Goldberg and Dallmeyer, 1997; Johnson et al., 2001).

The pegmatites vary in texture and mineralogy and range in size from less than 1 m to 200 m in width (Wood, 1996). The Spruce Pine pegmatites are chemically and mineralogically similar to the associated granodiorite plutons (Wood, 1996). The majority of Spruce Pine pegmatites are mineralogically simple, containing varying proportions of plagioclase (commonly oligoclase and albite), K-feldspar, quartz and muscovite. Some pegmatites, however, contain rare-element minerals such as beryl, tourmaline, fluorite, lepidolite, pollucite and columbite/tantalite (e.g. the Ray mine pegmatite, the McHone pegmatite, and the Crabtree pegmatite). As noted above, the Crabtree pegmatite forms an intrusive body emplaced between structurally lower chlorite schist and overlying quartz-mica schist (Figure 2). Exposures of the Crabtree pegmatite and host rocks are depicted on the mine map in figure 3. Amphibolite is exposed contiguous to the chlorite schist and structurally overlies the quartz-mica schist as isolated exposures.

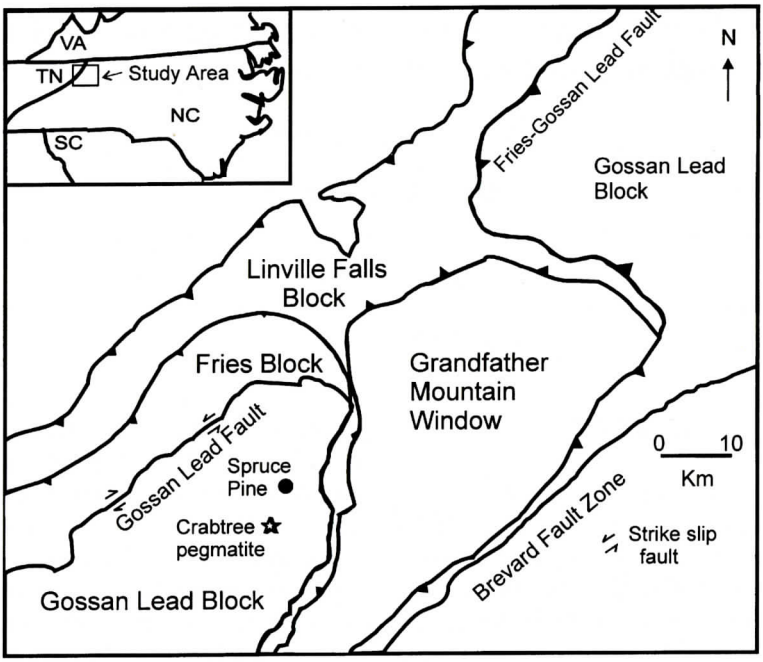

Figure 1. Thrust blocks of the Blue Ridge Belt. The Crabtree pegmatite intrudes the Gossan Lead block, which is comprised of the Ashe and Alligator Back metamorphic suites. Fault block names follow Raymond (1998).

vide a geologic and geochemical description of this important pegmatite.

The Crabtree pegmatite is located in the Gossan Lead Block of the Blue Ridge Belt, 7.5-km southwest of Spruce Pine, North Carolina (Figure 1). Country rocks around the pegmatite belong to the Ashe Metamorphic Suite and include chlorite schist, quartz-mica schist and amphibolite (Brobst, 1962; Abbott and Raymond, 1984; Brown et al., 1985; Tappen, 1998). The chlorite schist is present along the western contact of the pegmatite, whereas the quartz-mica schist is exposed in a zone along the eastern contact of the pegmatite. Amphibolite is exposed west of the chlorite schist and as isolated masses that occur structurally above the quartz mica schist.

GENERAL GEOLOGY

The Blue Ridge Belt is divided into the Western Blue Ridge Belt and the Eastern Blue Ridge Belt (Hatcher, 1978). The rocks of the Western Blue Ridge Belt are of Neoproterozoic North American (Laurentian) affinity. The Eastern Blue Ridge Belt contains allochthonous rocks representing a continental margin, seafloor sediments, and underlying oceanic crust (Hatcher, 1978; Abbott and Raymond, 1984; Raymond, 1998).

The structural units of the Blue Ridge Belt consist of a series of thrust blocks (Figure 1). The Crabtree pegmatite intrudes the easternmost block, the Gossan Lead Thrust Block, which overlies the Gossan Lead thrust fault (Figure 1). The Gossan Lead Block contains the Ashe and Alligator Back metamorphic suites (Rankin et al 1973; Abbott and Raymond, 1984; 1997). The Crabtree pegmatite intrudes the Ashe Metamorphic Suite. The Alligator Back Metamorphic Suite is exposed to the northeast of the Grandfather Mountain Window and locally to the southwest (Brown et al., 1985). The Ashe Metamorphic Suite, exposed widely both to the northeast and southwest of the Grandfather Mountain Window, is dominated by a mixture of plagioclase-hornblende schist and gneiss, pelitic schists, and quartz-feldspar semi-

Table 1. Representative modal composition of the host rock surrounding the Crabtree pegmatite.

Rock type	chlorite schist	mica schist	amphibolite
chlorite	30	3	0
actinolite	2	0	0
hornblende	0	0	74
plagioclase	36	10	18
k-feldspar	tr	tr	0
quartz	10	23	0
biotite	5	50	0
white mica	4	2	0
garnet	2	0	1
pyrite	2	1	0
apatite	3	3	0
titanite	3	3	6
rutile	tr	tr	tr
epidote	tr	0	0
zoisite	0	0	1
tourmaline	0	3	0
opaques	0	2	0
calcite	3	0	0
kyanite	0	tr	0
*Total	100	100	100

*Total = number of points counted

tr = trace amounts

ANALYTICAL METHODS

Optical petrographic methods were used to investigate the mineral identity of the host rock and pegmatite and to choose minerals suitable for chemical analysis. Modal data were collected by the optical point count method. Mineral compositions of beryl (green, yellow, and emerald), tourmaline, plagioclase, chlorite, biotite, and muscovite were determined using the Cameca SX-100 electron microprobe at the American Museum of Natural History. Beam conditions included a 20-micron diameter, 15 KeV acceleration potential for major elements and a 10 nA beam current. To acquire the trace elements, Cr, Cs, and Cl, a 40nA beam current was used. For acquiring boron in tourmaline, a 10 KeV accelerating potential and a 100 nA beam current was used. Counting times are 20 seconds (s) for major elements and Cl, 50 s for F and Cr, and 140 s for B. The SX-100 detection limit for B is 8000 ppm. The following standards were used for K σ X-ray lines: Na: albite; Si, Al, Ca: anorthite; K: orthoclase; Fe: fayalite; Mg: Wakefield diopside; Mn: rhodonite; Ti: synthetic TiO_2; P: berlinite; F: MgF_2; Cs: CsV_2O_5; Cl: scapolite; Cr: $MgCr_2O_4$; and B: Corning glass SRM93A.

Whole-rock and mineral separates were prepared at the Smithsonian Institution, where hand picked samples were washed, reduced in a jaw crusher to pea-sized particles, and ground to minus 200 mesh in an alumina-ceramic shatter box. X-ray fluorescence analysis (XRF) was conducted at Washington University (St. Louis, Missouri) for major- and trace element abundances of whole rock and mineral separates using procedures described by Dymek and Smith (1990). Trace elements analyzed include Sn, Nb, Zr, Y, Sr, Rb, Pb, Ga, Zn, Ni, V, Cr, Cs, Ba and Co. The trace element uncertainty is as follows: Nb, Zr, Y, Sr, Ga, $\pm$ 1 ppm; Zn, Sn $\pm$ 2 ppm; V, Ni, Pb $\pm$ 3 ppm; Ba $\pm$ 12 ppm; Cr $\pm$ 13 ppm; Cs $\pm$ 24 ppm.

HOST ROCK PETROLOGY AND GEOCHEMISTRY

Chlorite Schist

Dark green chlorite schist forms a ridge at the western contact of the pegmatite (Figures 2 and 3). The chlorite schist is dominated by chlorite but contains plagioclase, calcite, pyrite, titanite and actinolite. Table 1 shows the representative modal composition of the chlorite schist host rock. Accessory apatite, epidote, calcite and pyrite are dispersed throughout the matrix with occasional garnets and muscovite. Staining reveals the absence of K-feldspar. In plane-polarized light, chlorite occurs as light green plates, which are interleaved and impart a weak to strong foliation. The feldspars are commonly

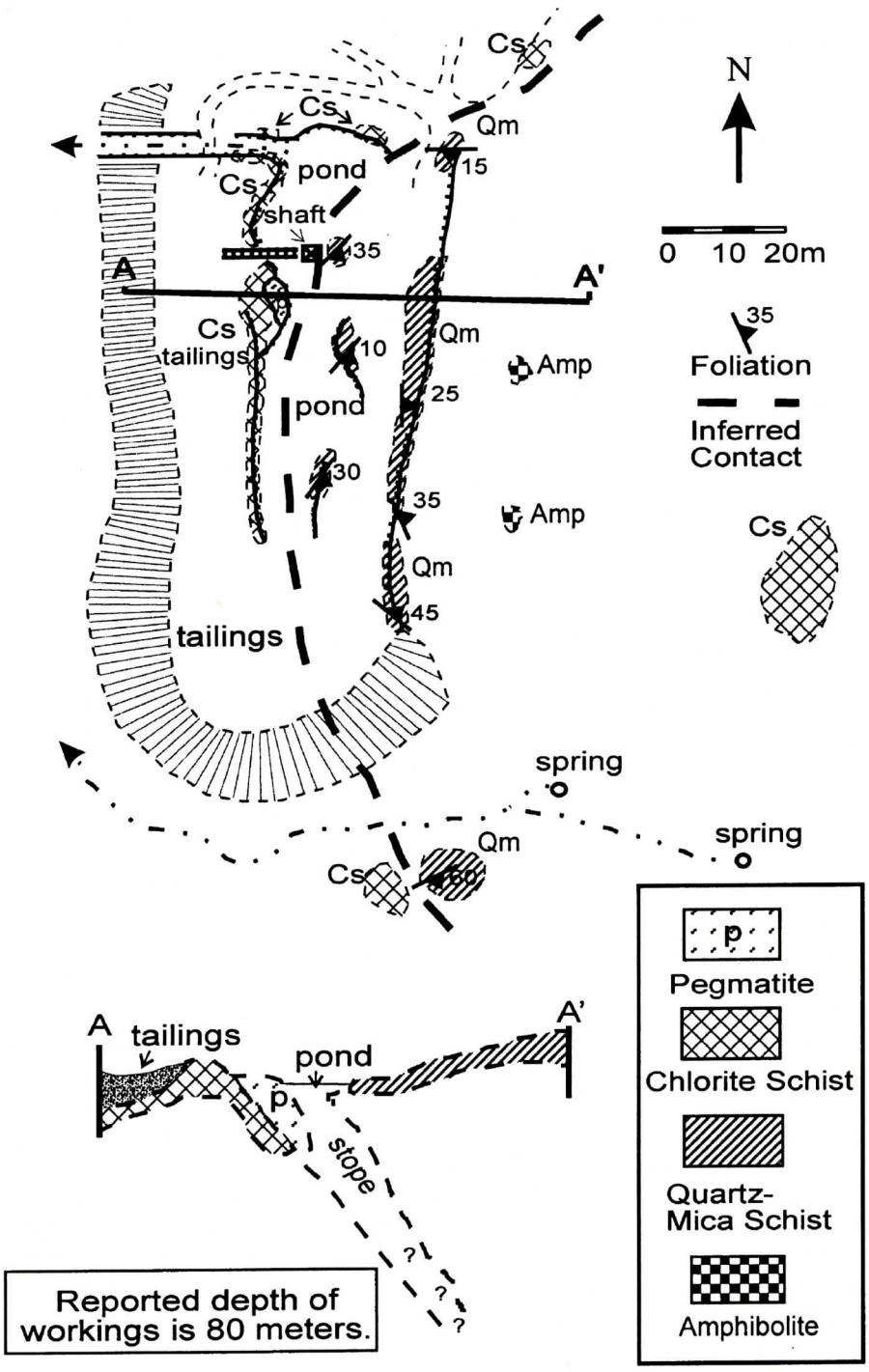

Figure 3. Mine map of the Crabtree pegmatite, Spruce Pine district, North Carolina showing the location of the host rocks and the pegmatite (courtesy J.A. Dockal). Amp=amphibolite; Cs = chlorite schist; p = pegmatite, Qm = quartz-mica schist.

Table 2. Major and trace element XRF whole rock data for the Crabtree host rock

Sample	EM97L	EM97N	CEM97-41	*NCC055	*Group II
Description	Crabtree qtz-mica schist	amphibolite	chlorite schist	mica schist and gneiss	amphibolite
SiO_2	69.38	50.18	67.94	43.50 - 70.40	49.31 - 53.16
TiO_2	0.63	1.81	0.79	0.96 - 1.30	1.01 - 1.88
Al_2O_3	13.40	15.14	13.50	12.00 - 29.90	13.93 - 16.20
FeO	n.d.	n.d.	n.d.	4.90 - 7.70	n.d.
Fe_2O_3	2.88	10.98	4.19	1.20 - 6.60	9.44 - 14.15
MnO	0.16	0.18	0.09	0.05 - 0.24	0.12 - 0.20
MgO	1.58	7.44	4.06	2.80 - 3.90	6.68 - 8.77
CaO	1.87	10.46	1.93	1.50 - 3.00	9.38 - 12.78
Na_2O	2.15	2.37	5.25	1.91 - 2.60	2.45 - 3.61
K_2O	2.45	0.30	0.37	1.10 - 3.70	0.12 - 0.53
P_2O_5	0.31	0.15	0.27	0.18 - 0.33	0.15 - 0.33
LOI	5.22	0.35	1.57	n.d.	n.d.
Total	100.02	99.36	99.95	101 - 100.83	98.38 - 100.23
Sn	<4.90	<5.20	6.20	n.d.	n.d.
Nb	19.60	8.60	16.70	<10.00 - 28.00	3.00 - 14.00
Zr	191.40	107.90	208.30	251.00 - 470.00	95.00 - 108.00
Y	34.40	33.30	21.70	27.00 - 71.00	22.00 - 51.00
Sr	115.90	182.00	91.70	115.00 - 500.00	100.00 - 188.00
Rb	74.10	<3.4	14.00	91.00 - 172.00	2.00 - 13.00
Pb	42.90	6.50	10.30	n.d.	n.d.
Ga	21.60	19.80	16.00	n.d.	n.d.
Zn	38.30	92.40	73.60	82.00 - 187.00	n.d.
Ni	49.10	39.70	20.80	23.00 - 68.00	45.00 - 76.00
V	75.10	294.70	59.80	n.d.	210.00 - 312.00
Cr	52.90	296.60	35.10	56.00 - 95.00	157.00 - 230.00
Cs	<20.0	<22.8	<19.4	<0.80 - 3.40	n.d.
Ba	644.80	47.90	119.20	490.00 - 770.00	n.d.
Co	24.50	20.80	14.50	13.40 - 49.00	n.d.

*Group II amphibolite from Misra and Conte(1991) Ashe Metamorphic Suite

Mica schist and gneiss from Lesure (1992), Buncombe and Yancy Counties, NC.

< = element concentration is below the detection limit of the analytical standard

n.d. = not determined

Trace element uncertainty is Nb, Zr, Y, Sr, Ga ± 1 ppm; Zn, Sn± 2 ppm;

V, Ni, Pb ± 3 ppm; Ba ± 12 ppm; Cr ± 13 ppm; Cs ± 24 ppm.

untwinned. Garnet (1.25 mm) is present as hypidioblastic, fractured crystals. Locally, chlorite partially or completely replaces garnet leaving a pseudomorphic outline. The mineralogy indicates that the rock reached the upper greenschist facies grade of metamorphism. Replacement of garnet by chlorite suggests that retrograde metamorphism has taken place.

Observations of outcrop and float samples show masses of chlorite enclosing coarse-grained porphyroclasts of quartz and plagioclase. The porphyroclasts range from 5 to 10 cm in length and 2 to 5 cm in width. They are typically elongate or irregularly ellipsoid with the long dimensions commonly parallel to the chlorite foliation. Fine-grained quartz grains form sigma-type pressure shadows around larger quartz grains of the porphyroclasts indicating recrystallization and shear during deformation. The plagioclase is An_{3-7}, consistent with greenschist facies metamorphism.

The whole-rock geochemistry of the host rocks is reported in Table 2. The quartz-plagioclase porphyroclasts of the chlorite schist dominate the bulk geochemistry of this rock type, which shows 5.25 % Na_2O, 1.93 % CaO, and 0.37 % K_2O. The CaO content may be attributed to the feldspars and accessory apatite. The molar ratio of $Al_2O_3/Na_2O + K_2O + CaO$ is 1.08 reflecting a peraluminous nature. Since chlorite dominates the matrix of this rock, it is likely to hold the ferromagnesian elements and the bulk of the trace elements (Nesse, 1991). Concentrations of Zr (208.30 ppm) and Ba (119.20 ppm) are markedly higher than the other trace elements. Zn (73.60 ppm) and Sr (91.70) have intermediate abundances, whereas Cr is low (35.10 ppm). The chlorite in the chlorite schist host rock is Mg-Fe rich with a Mg/Mg+Fe molar ratio of 0.65 to 0.70 (as determined by electron microprobe analysis - EMPA). The Cr content is very low, with values from 0 – 0.0013 atoms per formula unit (apfu). Rare actinolite has 0.004 (apfu) Cr.

Quartz-mica Schist

The quartz-mica schist can display a variety of textures and mineralogy; it is fine- to medium-grained and schistose to gneissose. In hand sample, biotite and muscovite plates produce a well-defined foliation. Red garnets occur locally. The mineralogy of this rock includes biotite, quartz, muscovite, plagioclase, K-feldspar, garnet, and pyrite, plus trace amounts of rutile, kyanite and tourmaline. Table 1 shows a representative mode. The plagioclase (An_{19-27}) typically exhibits albite twinning. Garnet occurs as: 1) hypidioblastic, fine (0.5 mm) crystals with minor, randomly oriented inclusions of quartz, plagioclase, and opaque minerals; and 2) coarse-grained, poikiloblastic crystals with fractures oriented perpendicular to the phyllosilicate foliation. The mineralogy is indicative of the middle amphibolite facies grade of metamorphism. The geochemistry of this schist in Table 2 shows major and trace element values similar to the mica schist and gneiss from Buncombe and Yancey Counties found by Lesure (1992). The Crabtree mica schist has 52.90 ppm Cr. Mica schist and gneiss from Lesure (1992) has 56.0 to 95.0 ppm Cr. However, in contrast, the Zr, Rb and Zn values in the Crabtree mica schist are slightly below those in the schist and gneiss analyzed by Lesure (1992). In the Crabtree muscovite and biotite, EMPA data show low Cr concentrations with up to 0.005 apfu. Biotite contains 0.2 to 0.3 apfu F.

Amphibolite

The amphibolite hand sample is dark green to dark gray in color with a distinct fine-grained lineation defined by the alignment of hornblende prisms. The mineralogy includes hornblende and plagioclase with accessory sphene, zoisite, garnet, quartz, and rutile. The plagioclase ranges from An_{36} to An_{50}. The garnets are hypidioblastic to idioblastic and fractured, but lack inclusion trails. The mineralogy is indicative of amphibolite-facies conditions of metamorphism. The chemistry is compared with data from amphibolites in the Ashe and Alligator Back metamorphic suites, northeast of the Grandfather Mountain Window, reported from Misra and Conte (1991). The Cr is 296 ppm in the Crabtree amphibolite and 157 to 230 ppm in the Group II amphibolites of Misra and Conte

Table 3. Distribution of tourmaline, beryl, plagioclase, quartz and phyllosilicates in the Crabtree pegmatite.

Location	Mineral	Description	Pleochroic colors of tourmaline
Chlorite schist exo-contact	dravite	dark brown crystals 0.5 mm-2 cm long	blue rims, yellow cores
	emerald/green beryl	0.4 mm - 1 cm long	
	chlorite	fine - medium flakes	
Biotite schist exo-contact	biotite	fine to medium flakes 0.5 mm - 1 cm long	
	dravite	dark brown crystals up to 2 cm long	dark yellow - blue rims, orange cores
	emerald/green beryl	0.4 mm - 5 cm long	
	quartz	fine grained, 1 - 5 mm	
chilled margin	albite	0.2 - 2 mm	
	quartz	0.2 - 2 mm	
core	dravite-schorl	up to 8 cm long	yellow rims, blue cores, patchy blue zonations
	emerald/green beryl	1 - 2 cm long	
	yellow beryl	3 - 10 cm long	
	aquamarine	1 - 3 cm long	
	albite	2 - 5 cm	
	quartz	2 - 5 cm	
xenolith	schorl	up to 2 mm long	dark blue rims, yellow cores
	albite	1 - 2 mm	
aplite	albite	0.5 - 2 mm	
	yellow beryl	10 - 20 mm long	

and characteristics of beryl, tourmaline, plagioclase, quartz and phyllosilicates in the Crabtree pegmatite and exocontacts. Emerald and tourmaline occur mainly in the alteration zones. Brown to black tourmaline is common splaying into the pegmatite margin in a comb texture or oriented with the long dimensions parallel with the pegmatite/host rock contact. Tourmaline also occurs as random "sunburst" patches in the pegmatite, and splays from the xenolith margins. As smaller crystals, emerald and green beryl occurs in the pegmatite margin in a matrix of albite and quartz. Yellow beryl occurs in the pegmatite margin, the pegmatite center, and as accessory phases near and in the resorbed xenoliths. Rare aquamarine occurs near the pegmatite margin. Green and purple fluorite was common at depth in the exposures visible before mine flooding (Ledford, personal communication, 1998). Purple fluorite forms as thin stringers in the pegmatite margin.

Garnet and muscovite are accessory minerals in the Crabtree deposit. The garnets, 3 mm in diameter, are highly fractured, and are located locally in the biotite schist exocontact and the pegmatite margin. Garnet chemistry lies in the almandine-spessartine end member series. The garnet from the pegmatite margin has 1.7 – 1.8 apfu Fe (tot), 0.60 apfu Mn, >0.30 apfu Mg and low Ca (0.1 apfu). Cr is very low, from 0 to 0.004 apfu. The muscovite has up to 0.3 apfu F and 0.3 apfu Mg. Na varies from 0.2 apfu to 0.8 apfu. Cr content is low from 0 to 0.003 apfu, typically, and the highest amount measured is 0.018 apfu.

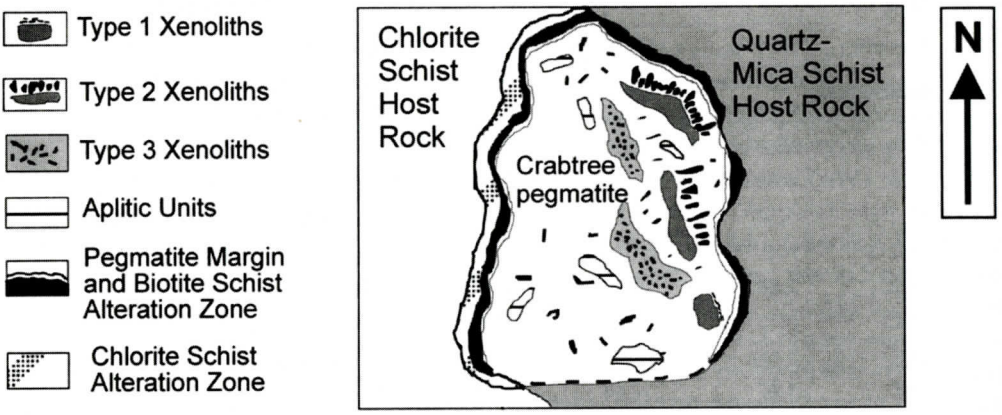

Figure 4. Schematic diagram of the Crabtree pegmatite in map view, depicting the xenoliths and aplitic units in the pegmatite, as well as the host rocks and alteration zones.

(1991, Table 2). Misra and Conte (1991) interpret the analyzed amphibolite to represent oceanic crust formed in a rift environment.

THE CRABTREE PEGMATITE

The Crabtree pegmatite is located 2.5-km northwest of Little Switzerland (7.5-km southwest of Spruce Pine) North Carolina at 82°7'20" longitude and 35°52'30" (Figure 2). The Crabtree emerald mine corresponds to mine number 691 recorded by Lesure (1968). After mining excavation, the surface exposure of the pegmatite is 5.4 m in length and 3.5 m in width. Figure 4 is a schematic diagram of the pegmatite surface in map view. The pegmatite has a north-south strike with a 55° E dip (based on the contact with the chlorite schist). The Crabtree pegmatite is a texturally unzoned, albite quartz pegmatite with an irregularly shaped chilled margin. Weakly developed textural variations occur as coarser grained segregations and aplitic units in randomly distributed patches. The chilled margin consists predominantly of plagioclase and quartz (0.2-1 mm), with local muscovite. Here the plagioclase is commonly untwinned and irregularly shaped. The plagioclase (An_{2-12}) and quartz grains dominating the pegmatite are relatively fine-grained, with sizes up to 1 cm. Between the country rock and the pegmatite there are two metasomatic contact reaction zones (biotite schist and chlorite schist) referred to as exocontacts. Emeralds in the biotite schist exocontact and the pegmatite margin have abundant quartz and rare plagioclase inclusions (0.25 to 0.5 mm in size). One plagioclase inclusion analyzed by EMPA, has a composition of An_9. Coarse-grained segregations contain plagioclase, smoky quartz and yellow beryl. The plagioclase is locally twinned and grains range up to 2 cm. The composition of plagioclase in coarse-grained segregations is An_{3-6}.

Randomly dispersed aplitic aggregates of plagioclase, quartz, yellow beryl and garnet are present throughout the pegmatite (Figure 4). The aplitic units are greater than 10 cm in length. The yellow beryls are fine-grained, with sizes ranging from 3 to 5 mm in diameter and up to 10-20 mm in length. Biotite schist xenoliths, which are abundant, show three types of progressive assimilation. In type 1 xenoliths, the inclusions retain their shape and show little deformation. The morphology of the type 2 xenoliths is irregularly curved with tourmaline splaying from the margins. In the resorbed xenolith (type 3), the plagioclase has euhedral, sharp faces and is commonly twinned. The crystals range in size from 0.5 mm to 5 mm and have a composition of An_{2-5}.

Intrusion of the pegmatite has resulted in metasomatic alteration of the host rocks, forming the contact reaction zones known as exocontacts. Table 3 shows the mineral distribution

Table 5. Representative electron microprobe data for minerals in the alteration zones.

mineral	tur	tur	tur	tur	biotite	chlorite	beryl
position	rim	core	rim	core			
location	chlschex	chlschex	biotschex	biotschex	biotschex	chlschex	chlschex
slide no.	42b1r	42b1c	trbt5r	trbt5c	10a3 bt	42bchl	42be
P_2O_5	0.03	0.02	0.00	0.02	0.02	0.00	0.00
SiO_2	36.84	37.24	35.62	35.36	39.51	27.66	64.67
TiO_2	0.45	0.58	0.30	0.33	0.58	0.06	0.05
B_2O_3	11.54	11.20	10.80	11.91	n.d.	n.d.	0.00
Al_2O_3	31.15	30.68	30.67	31.75	13.90	20.74	15.81
V_2O_3	0.02	0.00	n.d.	n.d.	n.d.	nd.	0.04
Cr_2O_3	0.12	0.47	0.28	0.07	0.04	0.48	0.23
MgO	9.14	8.93	8.39	7.98	17.35	21.60	1.69
CaO	1.31	1.27	0.64	0.51	0.01	0.00	0.01
MnO	0.02	0.03	0.17	0.10	0.33	0.32	0.00
FeO	4.51	3.93	5.44	5.79	11.68	16.30	0.29
Na_2O	2.15	2.37	2.50	2.63	0.09	0.02	1.46
K_2O	0.02	0.01	0.02	0.04	9.66	0.06	0.00
Cs_2O	0.00	0.00	n.d.	n.d.	n.d.	n.d.	0.05
NiO	n.d.	n.d.	n.d.	n.d.	0.02	0.09	n.d.
F	0.64	0.45	1.36	1.32	3.06	0.09	0.00
BeO*	n.d.	n.d.	n.d.	n.d.	n.d.	n.d.	9.34
O=F	-0.27	-0.19	-0.57	-0.55	-1.29	-0.04	0.00
Total-F	97.66	97.18	95.62	97.25	94.94	87.29	93.63
Formulae normalized to	29 O	29 O	29 O	29 O	22 O	28 O	18 O
Si	5.89	5.99	5.85	5.69	5.73	5.57	6.32
Al	5.87	5.82	5.93	6.02	2.38	4.92	1.82
B	3.18	3.11	3.06	3.31	n.d.	n.d.	2.20
Be	n.d.	n.d.	n.d.	n.d.	n.d.	n.d.	2.20
Ti	0.05	0.07	0.04	0.04	0.06	0.01	0.00
V	0.00	0.00	n.d.	n.d.	n.d.	n.d.	0.00
Cr	0.02	0.06	0.04	0.01	0.01	0.08	0.01
Ni	n.d.	n.d.	n.d.	n.d.	0.00	0.02	n.d.
Mg	2.17	2.14	2.05	1.91	3.75	6.48	0.25
Mn	0.00	0.00	0.02	0.01	0.04	0.06	0.00
Fe	0.60	0.53	0.75	0.78	1.42	2.75	0.02
Na	0.67	0.74	0.80	0.82	0.03	0.01	0.28
Ca	0.22	0.22	0.11	0.09	0.00	0.00	0.00
K	0.00	0.00	0.00	0.01	1.79	0.01	0.00
Cs	0.00	0.00	n.d.	n.d.	n.d.	n.d.	0.00
F	0.33	0.23	0.71	0.67	1.77	0.05	0.00

n.d. = not determined
* BeO calculated on the basis of 3.0 apfu
tur = tourmaline

Table 4. Representative modal variation in the Crabtree pegmatite margin, type 3 xenolith, aplitic unit and alteration zones.

Location	aplitic unit	type 3 xenolith	pegmatite margin	chlorite schist exocontact	biotite schist exocontact
plagioclase	87	75	53	10	5
quartz	10	10	17	16	5
beryl	2	0	14	3	2
tourmaline	tr	15	13	14	3
white mica	1	2	4	3	0
garnet	tr	0	0	0	tr
biotite	0	0	0	1	54
K-feldspar	0	0	0	6	3
chlorite	0	0	0	47	0
actinolite	0	0	0	tr	0
titanite	0	0	0	tr	0
Total	100	102	101	100	72

tr = trace amounts

Alteration Zones

The Crabtree pegmatite/host rock relations are shown schematically in map view, in figure 4. The contact of the pegmatite with the chlorite schist host rock at the western boundary is sharp and irregularly curved. At this contact, there are two alteration zones (exocontacts). The chlorite schist exocontact grades into a biotite schist exocontact inward toward the pegmatite. In field exposures, it appears that the biotite schist exocontact encases most of the pegmatite body, but some mine rubble reveals that locally, the chlorite schist zone is directly in contact with the pegmatite.

The biotite schist of the alteration zone ranges up to 3 cm thick, locally, and appears to encase the pegmatite (as shown in figure 4). Table 4 shows that biotite, quartz, plagioclase, and tourmaline are the dominant minerals with trace amounts of garnet. Vibrant, grass green emerald mineralization also occurs in this location. Emerald has abundant quartz and plagioclase inclusions typically 0.5 mm in size. Coarse biotite flakes define a schistose texture oriented parallel to the pegmatite/wall rock contact. The metasomatic biotite is Mg-rich with Mg/(Mg+Fe) molar ratios ranging from 0.60 to 0.73. The F content in biotite ranges from 0.60 to 1.77 apfu. The chlorite schist alteration zone rocks are dominated by fine-grained, dark green chlorite. In the chlorite foliation, tourmaline and emerald are oriented parallel to sub-parallel to the pegmatite body contact. The chlorite schist exocontact rock also contains quartz, tourmaline, beryl, plagioclase, titanite, white mica, K-feldspar, and biotite. Table 4 shows a representative mode for this rock. The chlorites are randomly oriented, and locally exhibit decussate textures. Microprobe data for minerals from the two alteration zones are presented in table 5. The chlorite in the chlorite schist exocontact has up to 0.55 wt % Cr_2O_3. The Mg-Fe ratio ranges from 0.65 to 0.70 atoms per formula unit (apfu). Tourmaline prisms vary in length from 0.1 mm to 1.5 mm. The pleochroic scheme of the tourmaline varies widely, commonly with repeating blue and yellow concentric zones. However, the larger crystals typically have blue rims and yellow-orange cores (Table 3). The smaller crystals tend to have blue cores and yellow rims. Larger crystals show more inclusions of quartz, plagioclase, titanite, and smaller tourmaline prisms. Emerald in the chlorite schist alteration zone is usually 0.4 mm to 1.3 mm in size and occurs in two habits: 1) idioblastic crystals with only biotite inclusions, and 2) hypidioblastic crystals with tourmaline, quartz, plagioclase, and biotite inclusions.

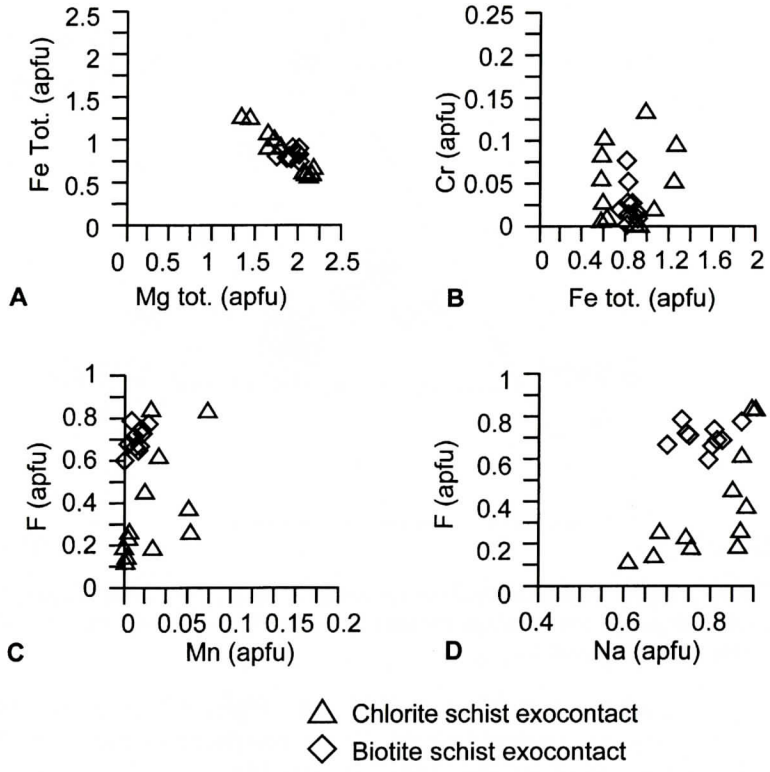

Figure 6. A. Fe vs. Mg in tourmaline from the chlorite schist and biotite schist exocontacts of the Crabtree pegmatite. Symbols for tourmaline are the same as denoted in figure 5. B. Cr vs. Fe for exocontact tourmaline. C. F vs. Mn for exocontact tourmaline. D. F vs. Na for exocontact tourmaline.

2.2 Mg apfu and 0.5 to 1.2 Fe apfu (Figure 6A). Cr concentration overall tends to be higher in tourmaline from this location with 0.14 apfu Cr (Figure 6B). In the biotite schist exocontact, the Cr concentration varies from 0 to 0.08 apfu. F ranges from 0.2 to 0.8 apfu in the chlorite schist and 0.6 to 0.8 apfu in the biotite schist, with low Mn concentrations (Figure 6C). Na ranges from 0.6 to 0.9 apfu (Figure 6D).

Margin and Xenolith Tourmaline

The dark brown to black tourmaline of the pegmatite margin, either splays into the pegmatite in a comb texture or is oriented with its long dimensions parallel to the pegmatite/host rock contact. Thin crystals, up to 0.5 cm in length, flare toward the pegmatite interior. Throughout the pegmatite body, tourmaline occurs in local aggregates of thicker prisms or "sunbursts" up to 5 cm in length. The crystals are brown or black and may be bent or fractured. Tourmaline in the pegmatite margin displays highly variable and diffuse pleochroic zoning colors (Table 3). The tourmaline commonly has blue cores with yellow rims, but may exhibit a patchy, irregular blue zonation. The larger tourmaline prisms are commonly 5 mm across and 7 mm in length. They are usually poikiloblastic and host quartz and untwinned plagioclase inclusions (0.25 mm - 0.5 mm). Tourmaline in the type 3 xenoliths are small, 1 to 2 mm in diameter and contain few to no inclusions. In thin section, they have yellow cores and blue rims, an opposite pleochroic zoning pattern to those in the margin. This pleochroic pattern is consistent in all of the tourmaline crystals, except in rare, smaller prisms that are entirely blue.

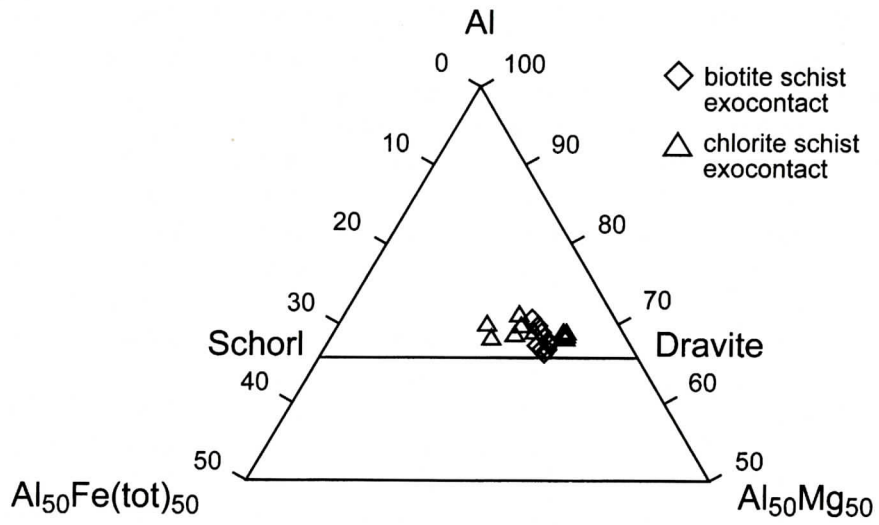

Figure 5. Al-Fe-Mg ternary diagram of tourmaline in the biotite schist and chlorite schist exocontact of the Crabtree pegmatite. The compositions are part of the dravite-schorl end member series. Diamonds represent tourmaline from the biotite schist exocontact and triangles represent tourmaline of the chlorite schist exocontact.

Xenoliths

Biotite schist xenoliths are concentrated mostly in the eastern half of the Crabtree pegmatite exposure (Figure 4). The xenoliths are generally oriented either parallel or sub-parallel to the biotite schist exocontact. Mineralogical and textural characteristics distinguish three types of biotite schist, and perhaps represent progressive assimilation of the inclusions. Type 1 xenoliths have a blocky morphology, showing little deformation. Biotite plates define the foliation. Tourmaline prisms are concentrated at the margins of the xenoliths, and are oriented parallel to the biotite foliation. In type 2 xenoliths, the phyllosilicates define the dominant exterior foliation, but the xenolith morphology is irregularly curved and rounded. Distinctive medium- to coarse-grained black tourmaline crystals, typically 2 to 7 cm in length, extend into the pegmatite from the margins of the xenolith, forming a comb texture. The tourmaline projects only toward the structural top of the pegmatite. The type 3 xenoliths occur as dark to light gray, tapered lenses. The xenoliths have long dimensions that are sub-parallel to parallel to the pegmatite/host rock contacts. The mineralogy of the type 3 xenoliths includes fine-grained albite, quartz, and black tourmaline. The tourmaline crystals are 2 mm in length and have orientations sub-parallel to one another.

TOURMALINE AND BERYL PETROGRAPHY (TEXTURES) AND CHEMISTRY

Exocontact Tourmaline

Tourmaline varies in size from 2.5 - 5 mm in basal section and 7 mm - 2 cm in length and has bright orange pleochroic cores and yellow to bluish rims (Table 3). Dark brown prisms are vitreous, euhedral and up to 1 cm in length and 0.5 cm in diameter. The tourmalines are oriented parallel to the biotite foliation. Poikiloblastic tourmaline commonly embays emerald crystals. Overall, the chemistry of tourmaline from both exocontacts is similar. Tourmaline microprobe compositions from both exocontacts are plotted in an AFM ternary diagram in figure 5. Tourmaline compositions from the chlorite schist exocontact are part of the dravite-schorl end member series (Table 5). The compositions are closer to the dravite member and have 1.4 to

Table 6. Microprobe data of representative tourmaline in the Crabtree pegmatite.

	sample location	cemh-6 xenolith rim	cemh-6 xenolith core	cem21-10 margin rim	cem21-10 margin core
	P_2O_5	0.06	0.01	0.00	0.02
	SiO_2	34.71	34.77	36.53	36.23
	TiO_2	0.14	0.12	0.50	0.60
	B_2O_3	10.41	10.44	11.75	11.00
	Al_2O_3	32.04	33.40	30.77	30.34
	V_2O_3	0.00	0.00	0.03	0.07
	Cr_2O_3	0.00	0.00	0.17	0.77
	MgO	3.84	1.00	8.42	8.38
	CaO	0.22	0.10	0.99	1.09
	MnO	0.67	0.52	0.08	0.10
	FeO	10.83	13.51	6.07	6.15
	Na_2O	2.43	1.91	2.45	2.45
	K_2O	0.04	0.04	0.02	0.02
	Cs_2O	0.07	0.04	0.01	0.00
	F	0.96	0.51	1.44	1.41
	O=F	-0.41	-0.21	-0.61	-0.59
	Total-F	96.02	96.04	98.61	98.63
T	Si	5.83	5.87	5.81	5.84
	Al	0.00	0.00	0.00	0.00
B	B	3.02	3.04	3.23	3.06
Z	Al	6.00	6.00	5.77	5.76
Y	Al	0.34	0.65	0.00	0.00
	Ti	0.02	0.02	0.06	0.07
	V	0.00	0.00	0.06	0.13
	Cr	0.00	0.00	0.21	0.10
	Mg	0.96	0.25	2.00	2.01
	Mn	0.07	0.06	0.01	0.01
	Fe	1.52	1.91	0.81	0.83
X	Na	0.79	0.63	0.76	0.77
	Ca	0.04	0.02	0.17	0.19
	K	0.01	0.01	0.00	0.05
		0.16	0.35	0.07	0.00
W	F	0.51	0.27	0.73	0.72
	Cs	0.01	0.00	0.00	0.00

n.d. = not determined

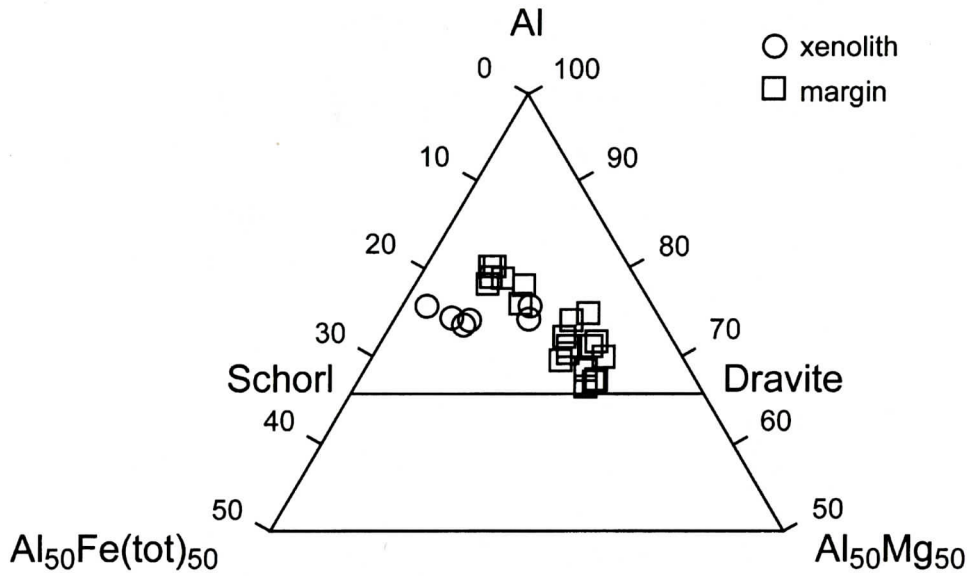

Figure 7. Al-Fe-Mg ternary diagram of tourmaline compositions in the Crabtree pegmatite margin and in the xenolith. Squares are symbols for tourmaline in the pegmatite margin and circles represent tourmaline from the xenolith.

Tourmalines associated with the Crabtree pegmatite have compositions intermediate to the dravite and schorl end members (Table 6). Figure 7 is an AlFeMg ternary plot of tourmaline chemistry from the Crabtree pegmatite margin and the type 3 xenoliths. The xenolith tourmaline compositions are closest to the schorl end member. Major-element chemistry of the tourmaline can be summarized as follows:

1. Like the tourmaline from the exocontacts, tourmaline in the pegmatite margin commonly has 0.5-1.2 apfu Fe. Tourmaline in the xenolith has high Fe with 1.0 – 2.0 apfu. Tourmaline in the pegmatite margin shows the largest variation in Fe concentrations (Figure 8A). Mg varies from 0.5 – 1.2 apfu in the xenolith and in the margin, Mg ranges from 0.5 to 2.1 apfu (Figure 8A).
2. Cr concentration tends to be very low in the margin and xenolith tourmaline (Figure 8B).
3. In the margin, F concentration varies from 0 to 0.8 apfu. F concentration in the xenolith varies from 0.2 to 0.6 apfu F. The Crabtree tourmaline has up to 0.16 apfu Mn. Figure 8C reveals that Mn is highest in margin tourmaline with 0.12 to 0.14 apfu Mn.
4. The Crabtree tourmalines are Na-enriched with values from 0.6 – 0.9 apfu (Figure 8D). Na and Ca show a positive correlation with F. The x site vacancy occupies 0.02 – 0.12 apfu in the tourmaline structure and rarely reaches 0.3 apfu.

The Fe-Mn substitution in minerals is a useful geochemical indicator for determining degree of fractionation in a pegmatite melt. Overall, the Mn concentration is very low (< 0.16 apfu) in the Crabtree tourmaline and does not show a Fe-Mn trend. However, there are two populations of margin tourmaline. One has high F and low Mn; the other has low F and high Mn (Figure 8C). The fluorine concentrations averaged from all points analyzed are moderate, ranging from 0.35 apfu in the chlorite schist exocontact, 0.41 apfu in the xenolith, and 0.51 apfu in the pegmatite margin, to 0.88 apfu in the biotite schist exocontact.

Beryl Petrology

In the Crabtree pegmatite mine, emerald and

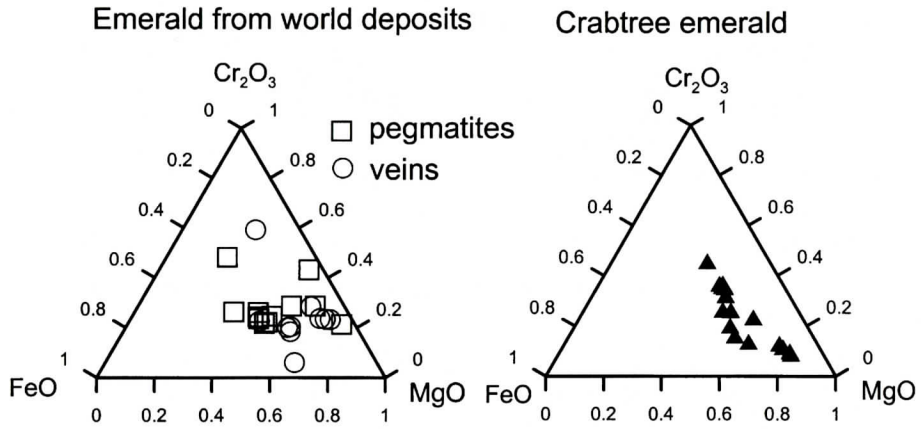

Figure 9. Cr_2O_3-FeO-MgO ternary diagrams comparing the Crabtree emeralds with emerald from pegmatite deposits and hydrothermal veins reported in the literature. Data for these deposits are compiled from Bank (1974), Graziani et al. (1983), Barros (1985), Hammarstrom (1989), Schwarz (1991), Aurisicchio et al. (1994) and Laurs (1995).

indication of the amount of Cr present (Hammarstrom, 1989). Wood and Nassau (1968) suggest that concentrations greater than 0.10% Cr_2O_3 are necessary to distinguish emerald from green beryl. In this study, beryl with less than 0.10% Cr_2O_3 and a pale green color is termed green beryl. Cr concentrations are roughly reflected by the color variation in the beryl. Pale, light green beryl from the Crabtree deposit contains 0.04 wt % to 0.13 wt % Cr_2O_3 whereas yellow beryl contains 0.00 - 0.03 wt % Cr_2O_3. Bright green emerald contains the highest Cr_2O_3 concentration ranging from 0.2 to 0.85 wt %. Along a traverse of a single emerald crystal, Cr_2O_3 concentration is variable. The chemical compositions of emerald are consistent with those of natural emeralds from other deposits (Figure 9). The chemical compositions of emeralds appear to be highly dependent on host rock compositions, and emeralds from the same occurrence show a wide chemical variation. The Crabtree emerald shows a well-defined trend. The emeralds show increasing FeO coupled with increasing Cr_2O_3 concentration.

The beryl associated with the Crabtree pegmatite is sodic (Table 7). The Crabtree beryl typically has 0.5 to 2-wt % Na_2O. Cerny (1975) shows that this chemistry is typical of beryls in pegmatites with albite-rich assemblages that are, at the same time, poor in rare alkalis. K_2O, CaO, MnO, and TiO_2 contents in Crabtree beryl are very low and vary between 0 and 0.05 wt %. Total FeO varies from 0.2 to 1 wt %. The FeO concentrations generally overlap between the emerald, green and yellow beryl. The MgO concentrations range from 0.20 to 2.3 wt %, with green beryl typically having values of 1.4 wt %.

Table 8 shows the mineral separate XRF data for the emerald, yellow beryl and aquamarine. Emerald contains significantly higher amounts of Cr (1564 ppm) and Cs (1066 ppm) than the other beryls. V, Rb, and Ni are also higher in the emerald than in the yellow beryl and aquamarine. MgO and Na_2O are higher in the emerald than in the green and yellow beryl, whereas Fe_2O_3 predominates in aquamarine. Interestingly, the Zn concentration is the highest for the aquamarine, which corresponds to the observation of Staatz et al. (1965), that zinc concentration is higher in beryl from pegmatite-related deposits than in beryl from any other environment. Staatz et al. (1965) also found that beryl in the host rock adjacent to the Harding (New Mexico) and Avon (Idaho) pegmatites contained greater amounts of V, Ti, Sc, Cr, Fe (total), Mg, Ni and Co than the beryl of the pegmatite. They suggest that these elements were largely obtained from the host rock. Higher concentrations of Fe_2O_3, MgO, Ni, Co, Cr and V in Crabtree emerald versus the Crabtree

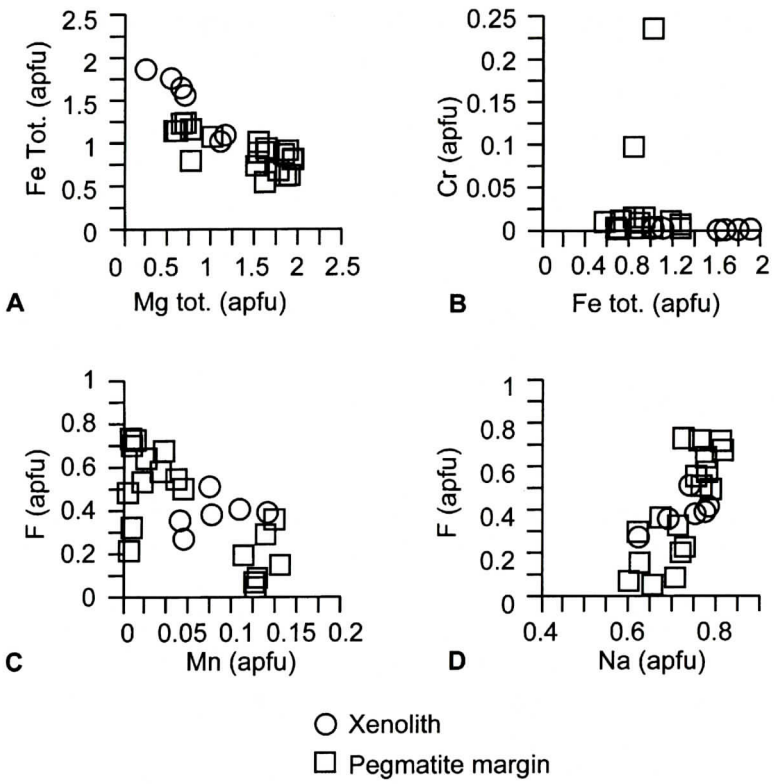

Figure 8. A. Fe vs. Mg in tourmaline from the xenoliths and Crabtree pegmatite margin. Symbols for tourmaline are the same as denoted in figure 7. B. Cr vs. Fe for pegmatite tourmaline. C. F vs. Mn for pegmatite tourmaline. D. F vs. Na for pegmatite tourmaline.

green beryl mainly occurs in the biotite and chlorite schist exocontacts and is less common in the pegmatite margin. The aquamarine and yellow beryls occur in the pegmatite. Yellow beryl also occurs in the xenoliths within the pegmatite. Emerald is oriented both normal and sub-parallel to the pegmatite contact and has vibrant grass green coloration. Light green beryl occurs as subhedral to euhedral pale green hexagonal prisms and generally occurs in a matrix of quartz and plagioclase. Green beryl commonly grades into yellow beryl along the length of prisms. Beryl crystals with yellow cores and green rims are also common in mine debris samples and pegmatite boulders. Rare aquamarine occurs as subhedral crystals with a pale blue color.

Thin sections reveal emerald in anhedral to subhedral crystals, with basal sections up to 1 cm in diameter. Dark green emerald hosts abundant, randomly oriented, tabular and rounded quartz and plagioclase inclusions (0.25 to 0.5 mm in size) with serrated crystal boundaries. The quartz and plagioclase inclusions host Mg-rich biotite flakes. Quartz and plagioclase inclusions also rarely host tourmaline that locally contains biotite inclusions. Green beryl occurs as subhedral to euhedral crystals with fewer quartz and plagioclase inclusions than the emerald. Green beryl also hosts biotite inclusions. Aquamarine is subhedral with minor fractures and is inclusion-free. The euhedral hexagonal prisms of yellow beryl range from 1 to 10 mm in diameter. The yellow beryl has thin fractures and contains minor inclusions of quartz and plagioclase.

Beryl Chemistry

The intensity of green color in emerald is an

Table 8. Major and trace element XRF data in weight % and ppm of Crabtree beryl.

Sample Beryl Type	CEM97-33.1 Yellow	CEM 97-33.2 Aquamarine	CEM97-33.3 Emerald
SiO_2	64.62	64.27	62.61
TiO_2	0.00	0.00	0.00
Al_2O_3	17.75	17.13	18.08
Fe_2O_3	0.30	1.43	0.66
MnO	0.02	0.03	0.01
MgO	0.41	0.6	1.62
CaO	0.15	0.01	0.04
Na_2O	0.92	0.87	1.25
K_2O	0.29	0.05	0.12
P_2O_5	0.00	0.00	0.00
BeO*	13.19	13.19	13.29
LOI	2.38	2.44	2.32
Total	100.03	100.02	100.00
Sn	4.60	5.30	4.50
Nb	2.70	<1.20	<1.00
Zr	2.40	1.70	37.70
Y	1.90	<1.10	3.10
Sr	3.30	<1.00	2.90
Rb	27.40	33.60	80.30
Pb	17.70	<4.90	8.80
Ga	27.20	20.60	22.10
Zn	94.50	140.10	79.40
Ni	<2.70	<2.70	32.40
V	6.40	4.30	56.40
Cr	16.30	18.40	1563.90
Cs	385.50	147.90	1065.70
Ba	34.20	<11.00	<21.70
Co	<4.70	<4.10	2.60

BeO* is calculated by difference
Trace element uncertainty is Nb, Zr, Y, Sr. Ga ± 1 ppm; Zn, Sn ± 2 ppm;
V, Ni, Pb ± 3 ppm; Ba ± 12 ppm;Cr ± 13 ppm; Cs ± 24 ppm.

Electron microprobe data for the chlorite in the chlorite schist host rock reveal up to 0.08 wt % Cr_2O_3. Samples of muscovite and biotite from the quartz-mica host rocks have up to 0.04 wt % Cr_2O_3. The chlorite in the chlorite schist exocontact has higher amounts of Cr with up to 0.55 wt % Cr_2O_3. Cr_2O_3 reaches 0.20 wt % in biotite in the biotite schist exocontact. The Cr (apfu) concentration is commonly slightly higher in chlorite schist exocontact tourmaline.

On the basis of the mineralogy (chlorite, actinolite, titanite, apatite, epidote), the protolith of the chlorite schist host rock is considered to be a mafic rock. The timing of the inclusion of the quartz-plagioclase porphyroclasts, either before or during metamorphism, is difficult to interpret. The chlorite schist host rock has chlorite pseudomorphically replacing garnet, indicating retrograde metamorphism. The retrograde mineral assemblage is most likely directly related to fluid metasomatism resulting from pegmatite intrusion (L.A. Raymond, personal communication, 2002).

Emerald occurs in distinct geologic environments. It occurs in 1) mafic and ultramafic zones in association with igneous rocks/pegmatites (Riverina deposit, Australia, Crabtree Deposit, N.C), 2) low temperature veins in sediments (Chivor and Muzo mines, Colombia) or metamorphic rock (Hiddenite, N.C.), and 3) the intercalation of Cr-enriched metavolcanic rocks and Be-enriched metapelites (Habachtal, Austria). The Crabtree deposit is a classic occurrence of emerald where mafic/ultramafic rock interacts with pegmatite during intrusion. At the Crabtree deposit, intrusion of a sodic magma into originally mafic resulted in interaction and migration of Cr from the chlorite schist into the pegmatite producing emerald during contact and regional metamorphism.

Pegmatite-Wall Rock Interactions and Element Mobility

Interaction between fluids derived from the pegmatite-forming magma and wall rock may modify chemical compositions of original primary mineral phases or convert the primary mineral assemblage into secondary assemblag-

yellow and green beryl suggests that they too were derived from the host rock.

DISCUSSION

Source of Cr for Emerald Formation

The Crabtree pegmatite magma intrudes mica schist and gneiss on the east and chlorite schist on the west. The mica schist and chlorite schist have 53 ppm and 35 ppm Cr, respectively (Table 2). The low Cr content of the chlorite schist host rock is likely the result of dilution of the bulk rock chemistry by the quartz-plagioclase porphyroclasts, but may result from overprinting by metasomatic metamorphism.

Table 7. Microprobe data of representative yellow beryl, green beryl and emerald in the Crabtree pegmatite.

Sample	10a3 - yellow beryl		21F - green beryl		sp3 - emerald	
	#1 - rim	#7 - core	#54 - rim	#59 - core	#64 - rim	#72 - core
SiO_2	65.80	65.35	66.27	66.34	66.72	70.26
TiO_2	0.00	0.00	0.01	0.00	0.00	0.00
Al_2O_3	17.44	16.46	16.64	16.46	17.24	14.89
V_2O_3	0.00	0.00	0.02	0.03	0.01	0.02
Cr_2O_3	0.00	0.00	0.11	0.02	0.68	0.52
Fe_2O_3	0.00	0.00	0.00	0.00	0.00	0.00
FeO	0.31	0.64	0.32	0.64	0.30	0.16
MnO	0.05	0.01	0.01	0.00	0.02	0.00
MgO	0.59	1.05	1.14	1.27	0.44	0.55
CaO	0.00	0.00	0.00	0.01	0.00	0.00
Na_2O	0.71	1.73	1.19	1.31	0.58	0.63
K_2O	0.00	0.01	0.01	0.01	0.00	0.00
P_2O_5	0.00	0.00	0.00	0.02	0.02	0.02
Cs_2O	0.04	0.00	0.00	0.02	0.07	0.02
BeO*	12.74	12.61	12.75	12.75	12.90	12.90
Total	97.68	97.86	98.47	98.89	98.98	99.97
	Formulae normalized to 18 anions					
Si	6.09	6.07	6.09	6.09	6.10	6.33
Al	1.89	1.80	1.80	1.78	1.86	1.58
Fe	0.02	0.05	0.03	0.05	0.02	0.01
Mg	0.08	0.15	0.16	0.17	0.06	0.07
Ca	0.00	0.00	0.00	0.00	0.00	0.00
Na	0.13	0.31	0.21	0.23	0.10	0.11
Ti	0.00	0.00	0.00	0.00	0.00	0.00
Mn	0.00	0.00	0.00	0.00	0.00	0.00
V	0.00	0.00	0.00	0.00	0.00	0.00
Cr	0.00	0.00	0.00	0.00	0.02	0.02
Be	3.00	3.00	3.00	3.00	3.00	3.00

* BeO calculated by stoichiometry; Be = 3 *apfu*

conditions occurs by complexing with fluoride, hydroxide, carbonate and chloride ligands (Brown et al., 1983, Wood 1992). The biotite has high F (1.7 apfu) concentrations in the quartz inclusions within an emerald suggesting that Be and fluoride complexing occurred. At Crabtree, rare fluorite stringers occur in the pegmatite margin and massive green and purple fluorite occurs in the exocontact. Similarly, Be-flouride complexing occurs at the Khaltaro deposit (northern Pakistan) where emerald mineralization is associated with fluorite at or near the pegmatite or vein contacts (Laurs et al., 1996). Be-fluoride complexes become unstable when the activity of fluorine decreases, which may be caused by precipitation of fluorite or topaz (Wood, 1992). Metasomatism of the chlorite schist host rock containing apatite, epidote, calcite, and actinolite liberated Ca for the fluorite precipitation.

CONCLUSIONS

The Crabtree pegmatite is texturally unzoned albite-quartz pegmatite with a weakly developed differentiation that includes randomly distributed aplitic units and coarser grained segregations. Biotite schist xenoliths, displaying various degrees of assimilation, are abundant in the pegmatite exposure. The mineralogy also includes beryl (emerald, green, aquamarine and yellow), tourmaline and fluorite mainly occurring in the metasomatic alteration zones and less frequently in the pegmatite margin. The Crabtree emerald in the exocontact has higher Rb, Cs and Na_2O concentrations than the yellow beryl in the pegmatite margin. Fluorine concentrations of tourmaline (dravite-schorl) are typically higher in the exocontact than in the pegmatite margin. This suggests that element mobility rather than fractionation caused the rare element distribution. High F values in biotite inclusions in emerald indicate that Be-F complexes transported the Be ion. The precipitation of fluorite destabilized the Be-F complexes, allowing beryl to crystallize.

The chlorite schist host rock is the source of Cr for the emerald. The chlorite schist is a complex rock type showing evidence of retrograde metamorphism and dominated by quartz-plagioclase porphyroclasts. These factors may explain the low Cr concentrations in the whole rock chemistry. The Crabtree pegmatite intruded into originally mafic schist during which fluids diffused into the host rock releasing Cr and became preferentially incorporated into the beryl, tourmaline and biotite. High Rb, Cs and Na_2O concentrations in the emerald suggest that it formed as a late stage mineral.

ACKNOWLEDGEMENTS

This research was supported by grants from the Department of Earth Sciences at the University of North Carolina at Wilmington and the North Carolina Geological Society to C. Tappen. The authors thank the reviewers L. A. Raymond, M.A. Wise, J.D. Webster, and R. Hatcher for encouraging comments and suggestions. The authors express their gratitude to Dr. J. A. Dockal for help with fieldwork and creating a detailed mine map. Field mapping assistance from Dr. D. E. Blake is also greatly appreciated. The authors extend appreciation and thanks to Dr. M. A. Wise for insightful discussions and many visits to the Crabtree emerald deposit. Thank you to C. W. Mandeville for help in acquiring boron electron microprobe data for the tourmaline.

REFERENCES CITED

Abbott, R.N., and Raymond, L.A., 1984, The Ashe Metamorphic suite, northwest North Carolina: metamorphism and observations on geologic history: American Journal of Science, v. 284, p. 350 - 375.

Abbott, R.N., and Raymond, L.A., 1997, Petrology of pelitic and mafic rocks in the Ashe and Alligator Back metamorphic suites, northeast of the Grandfather Mountain Window *in* Stewart, K.G., Adams, M.G., and Trupe, C.H., eds., Paleozoic Structure, Metamorphism, and Tectonics of the Blue Ridge of Western North Carolina, Carolina Geological Society 1997 Field Trip and Annual Meeting, p. 87-101.

Aurisicchio, C., Grubessi, O., Zecchini, P., 1994, Infrared spectroscopy and crystal chemistry of the beryl group: The Canadian Mineralogist, v. 32, p. 55 - 68.

Bank, H., 1974, The emerald occurrence of Miku, Zambia: The Journal of Gemology, v. 14, p. 8 - 15.

Barros, C., 1985, The chemistry of emeralds and associated beryl in the Poragatu deposit, Brazil: Memorias congreso Latinoamericano de geologia, v. 1, p. 415 - 424.

es, forming wall rock exomorphic aureoles (Shearer et al., 1986). Metasomatism of wall rock adjacent to granitic pegmatite is commonly characterized by alkali and B- enrichment. Mineral assemblages found in metasomatized wall rock may consist of biotite, phlogopite, quartz, plagioclase, tourmaline, beryl, fluorite, and holmquistite (Li-amphibole) (Jahns, 1952, Page et al., 1953, Heinrich, 1962, London, 1986, Shearer et al, 1984, 1986).

An example of pegmatite fluid metasomatism is provided by the Tip Top pegmatite of South Dakota. According to Shearer et al. (1984), fluids migrating from the Tip Top pegmatite affected the mica schist host rock in two episodes. First migration of B rich fluids altered the rocks and later influx of Cs, Rb and Li-bearing fluids accompanied evolution of the pegmatite magma. Evidence of the latter is provided by Li in biotite and tourmaline crystallization closer to the wall zone, plus Cs enrichment of wall zone feldspar (Shearer et al., 1984).

The Crabtree host rock has been similarly affected by boron and alkali metasomatism. B-enrichment of the pegmatite fluid is manifested in the tourmaline of the exocontacts and the pegmatite margin. Abundant biotite mineralization in the alteration halo and high Na_2O, Rb and Cs values in the exocontact emerald indicate alkali metasomatism. Exocontact minerals at the Crabtree deposit show textural evidence of fluid migration. Emerald contains quartz inclusions. These quartz inclusions have biotite microlites and rare tourmalines that contain biotite as well.

The amount of biotite in the exocontact and as inclusions in tourmaline and emerald suggest that biotite began forming immediately after pegmatite melt intrusion, with biotite extracting K from the melt. B exsolved from the pegmatite melt soon thereafter producing tourmaline in the exocontacts and the pegmatite margin. Si from the pegmatitic fluid or Si released from the breakdown of minerals in the host rock mineralized emerald with abundant inclusions of quartz. Emerald contains quartz inclusions at all the levels of mine workings (Furbish, 1972). Mg, Fe, Ca and Cr released from the chlorite schist during alteration facilitated crystallization of tourmaline, fluorite and emerald. The occurrence of tourmaline-rich border zones is interpreted to record an influx of ferromagnesian components from host rocks into a boron rich pegmatite (London, 1990).

During magmatic fractionation, elements such as Li, Cs, Mn, Rb, F, B and P are typically incorporated into late stage minerals, commonly found in the innermost zones within pegmatites (Cerny, 1991). Alkali content in beryl also increases from margin to the core of the pegmatite (Heinrich, 1953, Staatz, 1965, Cerny, 1991). At Crabtree, emeralds in the biotite and chlorite schist exocontacts have higher Na_2O, Cs, Rb, FeO (tot), MgO, Cr, Ni and V concentrations than the yellow beryl and aquamarine in the pegmatite. Alkali enrichment in the emerald suggests that it formed latest in the sequence of beryl mineralization. In this case, fractionation was not the sole cause of rare element distribution. As an analogue, alkali enrichment of beryl in mica schist around pegmatite veins occurred at the Riverina emerald deposit, near Menzies, western Australia (Garstone, 1981). Garstone (1981) attributed this to fluids that increased in alkali content during progressive pegmatite crystallization and produced late stage emerald. Garstone (1981) also suggested that emerald mineralization is dependent on the length of time that the Be-bearing solutions were in contact with the ultramafic host rock.

At the Crabtree pegmatite, fluid transport and the timing of fluid influx may be the cause of rare element variations. The tourmaline chemistry shows evidence of fluid transport. Tourmaline in the pegmatite margin has values from 0 to 0.80 apfu F, whereas tourmaline in the biotite schist exocontact has 0.60 to 0.80 F. According to London (1992) metasomatic assemblages in host rocks mirror the composition of the innermost zones of the adjacent rare-element pegmatite, indicating that fluids are expelled from pegmatites after they have fully crystallized. High alkali values in the emerald may also be attributed to acids in aqueous pegmatite fluids (H_3BO_3, HCl and HF) breaking down the sheet silicates and releasing alkali elements (Shearer et al., 1984).

Transport of Be^{2+} in low to high temperature

ginia; a study from the Blue Ridge across the Brevard fault zone to the Sauratown Mountains anticlinorium: American Journal of Science, v. 273-A, p. 1-40.

Raymond, L.A., 1998, Geology of the Blue Ridge Belt of Northwestern North Carolina *in*

Deposits and Landforms on the Piedmont Slopes of Roan, Rich, and Snake Mountains, Northwestern North Carolina and Northeastern Tennessee, Southeastern Friends of the Pleistocene 1998 Field Trip, p. 1 - 7.

Tappen, C., 1998, Beryl and tourmaline mineralization of the Crabtree pegmatite, Spruce Pine District, North Carolina: [M.S. Thesis]: Wilmington, North Carolina, The University of North Carolina at Wilmington, 115 pp.

Schwarz, D., 1991, Australian emeralds: Australian Gemologist, v. 17, p. 488 - 497.

Shearer, C.K., Papike, J.J., Simon, S.B., Laul J.C. and Christian R.P., 1984, Pegmatite/wallrock interactions , Black Hills, South Dakota: Progressive boron metasomatism adjacent to the Tip Top pegmatite: Geochimica et Cosmochimica Acta, v. 48, p. 2563 – 2579.

Shearer, C.K., Papike, J.J., Simon, S.B., and Laul, J.C., 1986, Pegmatite wall rock interactions, Black Hills, South Dakota: Interaction between pegmatite derived fluids and quartz-mica schist wall rock: American Mineralogist, v. 71, p. 518 – 539.

Sinkankas, J., 1981, Emerald and other beryls: Pennsylvania, Chilton, 665 p.

Snee, L.W., and Kazmi, A.H., 1989, Origin and classification of Pakistani and world emerald deposits *in* Kazmi, A.H., and Snee, L.W., eds., Emeralds of Pakistan: Geology, gemology and genesis: New York, Van Nostrand Reinhold, p. 229 - 236.

Staatz, M.H., Griffits, W.R., Barnett, P.R., 1965, Differences in the minor element composition of beryl of various environments: American Mineralogist, v. 50, p. 1783 - 1795.

Wiener, L.S., and Merschat, C.E., 1990, Field guidebook to the geology of the Central Blue Ridge of North Carolina and the Spruce Pine mining district: North Carolina Geological Survey, Division of Land Resources, 24 p.

Wood, D.L., and Nassau, K., 1968, Infrared spectra of foreign molecules in beryl: American Mineralogist, v. 53, p. 777 - 800.

Wood, P.A., 1996, Petrogenesis of the Spruce Pine pegmatites, North Carolina: [M.S. Thesis]: Blacksburg, VA., Virginia Polytechnic Institute and State University, 99 p.

Wood, S.A., 1992, Theoretical prediction of speciation and solubility of beryllium in Hydrothermal solution to 300°C at saturated vapor pressure: Application to bertrandite/phenakite deposits: Ore Geology Reviews, v. 7, p. 249-278.

Brobst, D.A., 1962, Geology of the Spruce Pine district, Avery, Mitchell and Yancey Counties, North Carolina: U.S. Geological Survey Bulletin 1122-A, 26p.

Broughton, P.L., 1974, Emerald deposits of western North Carolina: Earth Science, v. 27, p. 222 - 228.

Brown, P.L., Ellis, J. and Sylva, R.N. 1983, The hydrolysis of metal ions, 7, Beryllium II: Journal of Chemical Society, Dalton Transactions. p. 2001-2004.

Brown, Z.A., Aruscavage, P.J., Brown, F.W., Mei-Leung, Hearn P.P., Philpotts, J.A., 1985, Some compositional aspects of Mesozoic diabase sheets from the Durham area, North Carolina *in* Robinson G.R, and Froelich A.J. (eds), Proceedings of the Second U.S. Geological Survey workshop on the early Mesozoic basins of the Eastern United States: Virginia: U.S. Geological Survey, p. 103 – 106.

Cerny, P., 1975, Alkali variations in pegmatitic beryl and their petrogenetic implications: Neus Jahrbuch feur Mineralogie Abhanlungen, v. 123, p. 198 - 212.

Cerny, P., 1991, Rare-element granitic pegmatites Part 1: Anatomy and Internal evolution of pegmatite deposits: Geoscience Canada, v. 18, p. 49 - 81.

Dymek, R.F., and Smith, M.S., 1990, Geochemistry and origin of Archaean quartz-cordierite gneisses from the Godtabsfjord region, West Greenland: Contributions to Mineralogy and Petrology, v. 105, p. 715 - 730.

Furbish, W., 1972, Unusual quartz inclusions in North Carolina emerald: Gems and Gemology, v. 14, p. 34-37.

Garstone, J.D., 1981, The geological setting and origin of emerald deposits at Menzies, Western Australia: Journal of the Royal Society of Western Australia, v. 64, p. 53 – 64.

Goldberg, S.A., and Dallmeyer, 1997, Chronology of Paleozoic metamorphism and deformation in the Blue Ridge thrust complex , North Carolina and Tennessee: American Journal of Science, v. 297, p. 488 - 526.

Graziani, G., Gubelin, E., Lucchesi, S., 1983, The genesis of an emerald from the Kitwe District, Zambia: Neues Jahrbuch fur Mineralogie, Monatschefte, v. 4, p. 175 - 186.

Hammarstrom, J.M., 1989, Mineral chemistry of emeralds and some associated minerals from Pakistan and Afghanistan: An electron microprobe study *in* Kazmi, A.H., Snee, L.W., eds., Emeralds of Pakistan: Geology, gemology and genesis, New York: Van Nostrand Reinhold, p. 125 - 150.

Hatcher, R.D., 1978a, Tectonics of the western Piedmont and the Blue Ridge, southern Appalachians: Review and speculation, American Journal of Science, v. 278, p. 276-304.

Heinrich, E.W., 1953, Zoning in pegmatite districts: American Mineralogist, v. 38: 1-2, p. 68-87.

Heinrich, E.W., 1962, Pegmatites in Rhys Sweden – examples of fluorite exomorphism: American Mineralogist, v. 47, p. 924 – 931.

Jahns, R.H., Griffitts, W.R., and Heinrich, E.W., 1952, Mica Deposits of the Southeastern Piedmont, Part I, General Features, U.S.G.S. Professional Paper 248-A 99 p.

Johnson, B.S., Miller, B., and Stewart, K., 2001, The nature and timing of Acadian deformation in the Southern Appalachian Blue Ridge constrained by the Spruce Pine Plutonic Suite, Western North Carolina: Geological Society of America Abstracts with Programs, v. 33, p. 30.

Kazmi, A.H., and Snee, L.W., eds., 1989, Emeralds of Pakistan: Geology, gemology and genesis: New York, Van Nostrand Reinhold Company, 269 p.

Kish, S.A., 1989, Paleozoic thermal history of the Blue Ridge in southwestern North Carolina – constraints based upon mineral cooling ages and the ages of intrusive rocks: Geological Society of America Abstracts with Programs, v. 21, p. 45.

Laurs, B.M., 1995, Emerald mineralization and amphibolite wall-rock alteration at the Khaltaro pegmatite-hydrothermal vein system, Haramosh mountains, northern Pakistan: [M.S., Thesis], Oregon, Oregon State University, 131p.

Laurs, B.M., Dilles, B.M. and Snee, L.W., 1996, Emerald mineralization and metasomatism of amphibolite, Khaltaro granitic pegmatite-hydrothermal vein system, Haramosh Mountains, Northern Pakistan: The Canadian Mineralogist, v. 34, p. 1253-1286.

Laurs, B.M., Dilles, J.H., Wairrach, Y., Kausar, A.B., and Snee, L.W., 1998, Geological setting of symmetrically zone, miarolitic granitic pegmatites at Stak Nala, Nanga Parbat-Haramosh massif, northern Pakistan: The Canadian Mineralogist, v. 36, p. 1 - 47.

Lesure, F.G., 1968, Mica deposits of the Blue Ridge in North Carolina: U.S. Geological Survey Professional Paper 577, 124 p.

Lesure, F.G., 1992, Whole-rock and trace-element analyses of some alumina rich gneiss and schist from the Blue Ridge, North Carolina and Georgia: U.S. Geological Survey Open-File Report 92-429, 4 p.

London, D., 1986, Holmquistite as a guide to pegmatitic rare metal deposits: Economic Geology, v. 81, p. 704 – 712.

London, D., 1990, Internal Differentiation of rare-element pegmatites; A synthesis of recent research *in* Eds., Hannah. J.L., and Stein, H.J., Ore-bearing Granite Systems; Petrogenesis and Mineralizing Processes, Geological Society of America Special Paper 246, p. 35 – 50.

London, D., 1992, The application of experimental petrology to the genesis and crystallization of granitic pegmatites: The Canadian Mineralogist, v. 30, p. 499-540.

Misra, K.C, and Conte, J.A., 1991, Amphibolites of the Ashe and Alligator Back Formations, North Carolina: Samples of late Proterozoic-early Paleozoic Oceanic Crust: Geological Society of America Bulletin, v. 103, p. 737 – 750.

Nesse, 1991, Introduction to Optical Mineralogy: New York, Oxford University Press, 333 p.

Page, L.R., et al., 1953, Pegmatite Investigations 1942 – 1945: U.S.G.S. Professional Paper 247, I-228.

Rankin, D.W., Espenshade, G.H., and Shaw, K.W., 1973, Stratigraphy and structure of the metamorphic belt in northwestern North Carolina and southwestern Vir-

SOUTHEASTERN GEOLOGY
V. 41, No. 4, March 2003, p.225 -228

ISOLATED AREAS OF PULPIT ROCKS ON THE LOOKOUT MOUNTAIN SYNCLINAL RIDGE: POSSIBLE ORIGIN AND DEVELOPMENT

CARL R. FROEDE JR.

U.S. Environmental Protection Agency, Region 4, Atlanta, Georgia 30303-8960, USA

A. JERRY AKRIDGE

Sypris Data Systems, 3322 S. Memorial Pkwy., Suite 505, Huntsville, Alabama 35801, USA

ABSTRACT

The Lookout Mountain synclinal ridge is capped by layers of silica-, carbonate-, and siderite-cemented Pennsylvanian-age Pottsville sandstone strata and quartz-pebble conglomerates. The uppermost exposed sandstone layer is case-hardened and displays extensive jointing. In certain places, the joints extend deeply into the underlying quartz-pebble conglomerates and sandstone layers, creating preferential pathways for erosion. Pulpit rocks have formed where a massive well-cemented, monogenetic, case-hardened sandstone cap has protected an underlying less-lithified mixture of quartz-pebble conglomerate and sandstone layers from weathering and erosion. These features are of varying sizes and occur in isolated areas on the top of the Lookout Mountain ridge.

INTRODUCTION

The Lookout Mountain synclinal ridge extends from Gadsden, Alabama, through northwest Georgia to Chattanooga, Tennessee. It is approximately 127 kilometers in length and extends northeastward at N30°E (Figure 1). The structure generally pinches toward the southwest as it moves from the Appalachian Plateaus Province to the Western Valley and Ridge Province (Akridge and Froede, 1998). The ridge increases in elevation as it moves northeast and stands 300 to 500 meters above the adjacent valley floors (Sullivan, 1942).

Capping the Lookout Mountain ridge is the Pennsylvanian-age Pottsville Formation. According to Alabama geologists, the Pottsville is relatively undifferentiated and described as a light-gray, thin- to thick-bedded quartzose sandstone and conglomerate containing interbedded dark-gray shale, siltstone, and coal (Raymond, Osborne, Copeland, and Neathery, 1988; Szabo, Osborne, Copeland, and Neathery, 1988). However, field mapping of the Lookout Mountain synclinal ridge conducted in the 1980s in Georgia indicates that the Pottsville sandstone layers can be subdivided, with pulpit rocks originating from the Warren Point Sandstone Member of the Gizzard Formation (Crawford, 1989). We noted that sandstone lay-

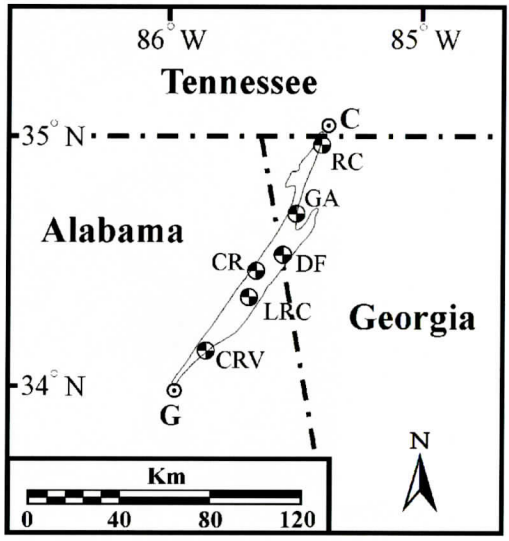

Figure 1. The Lookout Mountain synclinal ridge extends over three states in the southeastern United States. The general locations of some of the pulpit rocks identified as part of this investigation are noted (see Table 1 for more information). The cities of Chattanooga (C) and Gadsden (G) are indicated on the map.

Table 1. Location, global positioning system coordinates, and description of the pulpit rocks identified in this article

Location	Map Key	Latitude	Longitude	Description
Rock City, GA	RC	N 34° 58.373	W 85° 20.944	Isolated Pulpit Rock Column
GA Hwy 157	GA-1	N 34° 38.843	W 85° 28.233	Two Pulpit Rock Columns
	GA-2	N 34° 38.875	W 85° 28.221	Linear Pulpit Rock Wall
DeSoto Falls State Park, AL	DF-1	N 34° 29.816	W85° 37.100	Single Pulpit Rock with developing adjacent blocks
	DF-2	N34° 30.336	W85° 36.928	Howard Chapel Pulpit Rock
	DF-3	N34° 30.360	W85° 36.869	Isolated Pulpit Rock Column
Little River Canyon National Preserve, AL	LRC	N34° 22.457	W85° 37.891	Isolated Pulpit Rock Column
Citadel Rocks	CR	N34° 28.495	W85° 40.218	An area of developing pulpit rocks
Cherokee Rock Village	CRV-1	N34° 12.144	W85° 46.852	Large Pulpit Rock Wall
	CRV-2	N34° 12.119	W85° 46.866	Large Pulpit Rock Column
	CRV-3	N34° 10.840	W85° 49.017	Linear Pulpit Rock Wall

Once exposed to erosion, the underlying less-lithified quartz-pebble conglomerates and sandstone layers were rapidly weathered away. Loss of underlying support caused the massive sandstone cap rock to collapse and ultimately erode away. The pulpit rocks occur in areas where the massive sandstone cap rock remains intact and the underlying strata of less-lithified conglomerate and sandstone were not removed. While we view the age of the pulpit rocks as enigmatic, we do not interpret these somewhat delicate features as having withstood 300 million years of erosion.

THE SIZE AND SHAPE OF PULPIT ROCKS

The size and shape of the pulpit rocks reflect variations in the four factors previously noted. The tallest features occur in areas of greatest topographic relief and are associated with less-lithified strata of quartz-pebble conglomerate and sandstone. The dimensional arrangement of the joint sets extends vertically through the sandstone cap rock into the underlying quartzose strata. These deeply penetrating joints establish the length and width of each pulpit rock

Figure 3. The pulpit rock on the left is fully formed while the other blocks are still developing. Preexisting joints constrain their dimensions (Location DF-1).

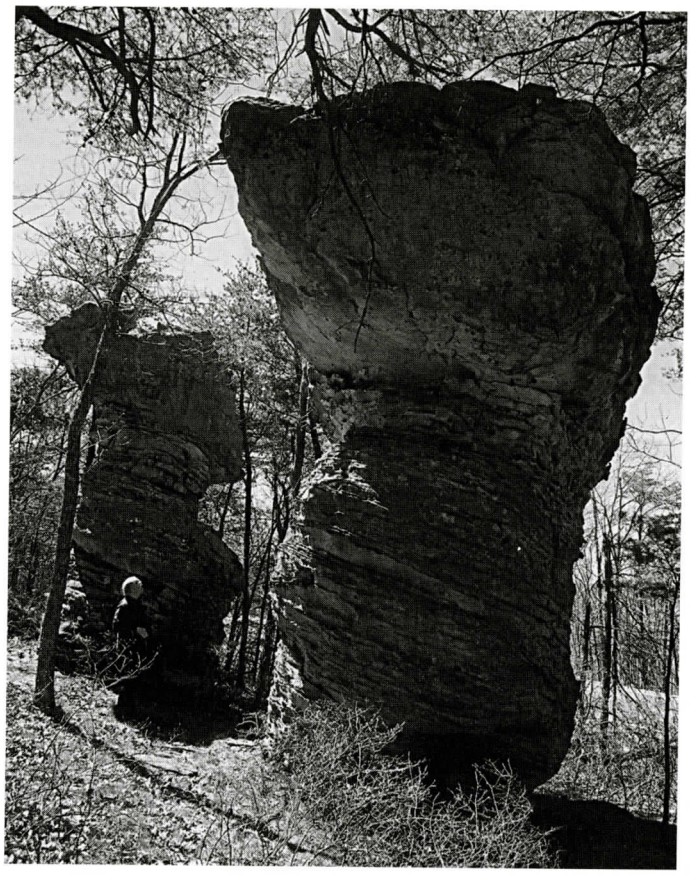

Figure 2. These pulpit rocks formed in an area of significant topographic relief (Location GA-1).

ers within the study area were primarily cemented by silica with some minor carbonate while the quartz-pebble conglomerates were predominately cemented by silica and siderite. All of the pulpit rocks that we observed are composed of layered sandstones and quartz-pebble conglomerates. They are best developed where a massive case-hardened well-cemented sandstone layer caps less-lithified strata composed of cross-bedded quartz-pebble conglomerate and sandstone (Figure 2).

For the purposes of this investigation we limited our fieldwork to the top of the Lookout Mountain syncline. Pulpit rocks might be present on adjacent ridges or knobs (e.g., Sand Mountain, Fox Mountain, Rock Mountain, and Pigeon Mountain) where the Warren Point Member of the Gizzard Formation is present and conditions existed that promoted their formation and development.

A PROPOSAL FOR THE ORIGIN OF PULPIT ROCKS

The pulpit rocks identified during this investigation formed at various locations on the Lookout Mountain synclinal ridge (Table 1). We attribute their formation and development to the interplay of four factors: 1) a localized steep topographic gradient, 2) a massive case-hardened well-cemented monogenetic sandstone cap rock, 3) less-lithified and poorly cemented mixtures of quartz-pebble conglomerate and sandstone layers, and 4) extensive deep-penetrating jointing.

We propose that the pulpit rocks formed due to overland flow eroding along well-developed joint sets in the massive sandstone cap rock.

Figure 4. This pulpit rock has been incorporated into the front of a church (Location DF-2). The large feature developed along joint sets within the sandstone and underlying conglomerate.

(Figure 3). We observed that these unique features range in size from one to six meters in elevation. Shapes vary from isolated columns to walls in their lateral expression. In one instance, a rather large pulpit rock is incorporated into the front of a small chapel (Figure 4). We also noted several locations within the area of investigation that contain joint-constrained blocks of strata that appear to be developing into pulpit rocks.

CONCLUSIONS

Pulpit rocks occur at several isolated locations on top of the Lookout Mountain synclinal ridge. They are possibly not limited to this ridge alone, but could extend to adjacent ridges and knobs if the stratigraphy and proper conditions allowed for their formation and development. The Pennsylvanian-age Pottsville Formation exposed atop the ridge is a massive cross-bedded sandstone that in places caps and protects underlying less-lithified strata composed of cross-bedded quartz-pebble conglomerate and sandstone from erosion. Extensive deeply-penetrating jointing within the Pottsville has enhanced erosion into the underlying softer strata. The removal of most of the less-lithified conglomerate and sandstone layers along with the overlying sandstone cap rock has resulted in the formation of isolated pulpit rocks.

ACKNOWLEDGMENTS

We thank Emmett L. Williams for his field assistance and helpful review of this article. This article does not necessarily represent the views or opinions of the U.S. Environmental Protection Agency, nor was this investigation conducted in any official capacity. Any mistakes are the responsibility of the authors.

REFERENCES

Akridge, A.J., and Froede, C.R., Jr., 1998, The general stratigraphy, paleontology, and geomorphology of DeSoto Falls and Little River Canyon, *in* Froede, C.R., Jr., ed., Big Ridge road cut, DeSoto Falls, and Little River Canyon, Northeastern Alabama: Spring field trip guidebook for the U.S. EPA Region 4 Geological Society, Atlanta, p. 16-21.

Crawford, T.J., 1989, Geology of the Pennsylvanian system of Georgia: Geologic Atlas #2, Atlanta, GA.

Raymond, D.E., Osborne, W.E., Copeland, C.W., Jr., and Neathery, T.L., 1988, Alabama stratigraphy: Geological Survey of Alabama, Circular 140, Tuscaloosa, AL.

Sullivan, J.W., 1942, The geology of the Sand – Lookout Mountain Area: northwest Georgia: Georgia Department of Natural Resources, Information Circular 15, Atlanta, GA.

Szabo, M.W., Osborne, W.E., Copeland, C.W., Jr., and Neathery, T.L., 1988, Geological map of Alabama: Geological Survey of Alabama, Special Map 220, Tuscaloosa, AL.

SOUTHEASTERN GEOLOGY
Duke University
Box 90233
Durham, NC 27708-0233

Returned Service Requested

Non-Profit Org.
U. S. POSTAGE
PAID
Durham, NC
Permit No. 60